# Thermal Properties of Asymmetric Nuclear Matter

A. Fedoseew[1] and H. Lenske[1,2]

[1] *Institut für Theoretische Physik, Universität Gießen Heinrich-Buff-Ring 16, D-35392 Gießen, Germany*
[2] *GSI Helmholtzzentrum für Schwerionenforschung, Planckstraße 1, 64291 Darmstadt, Germany*

(Dated: March 3, 2015)

The thermal properties of asymmetric nuclear matter are investigated in a relativistic mean-field approach. We start from free space NN-interactions and derive in-medium self-energies by Dirac-Brueckner theory. By the DDRH procedure we derive in a self-consistent approach density-dependent meson-baryon vertices. At the mean-field level, we include isoscalar and isovector scalar and vector interactions. The nuclear equation of state is investigated for a large range of total baryon densities up to the neutron star regime, the full range of asymmetries $\xi = Z/A$ from symmetric nuclear matter to pure neutron matter, and temperatures up to $T \sim 100$ MeV. The isovector-scalar self-energies are found to modify strongly the thermal properties of asymmetric nuclear matter. A striking result is the change of phase transitions when isovector-scalar self-energies are included.

PACS numbers: 21.10.-k, 21.30.-x, 21.65-f, 21.30Fe, 23.20.-g,21.60-n

arXiv:1407.2643v3 [nucl-th] 1 Mar 2015

## I. INTRODUCTION

A major task of nuclear many-body theory is to understand the equilibrium properties of nuclear matter under variations of density, pressure, proton-to-neutron fraction, and, last but not least, temperature. For this demanding goal decade-long experimental and theoretical efforts have been made, ranging from early studies of compound nuclei and highly excited pre-compound systems to studies of exotic nuclei at extreme isospin and compressed baryonic matter in high energy heavy ion collisions. Considering the status of research on the nuclear equation of state (EOS) one finds that many theoretical studies exist for symmetric and pure neutron matter. The work of Sauer *et al.* [1] is probably the first systematic study to derive the thermal properties of finite nuclei on theoretical grounds. Actually, historically nuclear matter studies were strongly motivated by astrophysical issues [2], with a especial need for investigations of asymmetric matter with arbitrary values of the charge asymmetry defined in terms of the proton fraction $\xi = \frac{Z}{A}$, ranging from $\xi = \frac{1}{2}$ in symmetric matter to $\xi = 0$ for pure neutron matter. Thermodynamically, symmetric nuclear matter and pure neutron matter, respectively, correspond to to single fluid systems. Since in symmetric nuclear matter isovector self-energies are absent by symmetry reasons, protons and neutrons are dynamically indistinguishable, hence forming a single-component fluid. The one-component character of neutron matter is obvious. The theoretical description of such one-component quantum systems is much simpler than that of a multi-component fluid. As is well known and will be seen also in later sections of this work, the treatment of asymmetric nuclear matter requires first of all extended theoretical methods and secondly such a two-fluid systems shows new features which are absent (or hidden by symmetry reasons) in a single-fluid nuclear matter.

Equilibrium thermodynamics, as pursuit here, is the appropriate approach to the nuclear equation of state as a function of density and temperature. Known essential properties are the liquid-gas phase transition at sub-saturation densities and moderate temperatures. An important question is how the system evolves by passing various *binodals*, denoting phase separation boundaries, and *spinodals*, indicating stability or, likewise, instability boundaries. Studies of infinite and finite nuclear systems indicate that symmetric nuclear matter undergoes a liquid-gas phase transition at critical temperatures in the range of $T_C = 10 \cdots 20$ MeV [2, 3]. The results depend, however, on the chosen $NN$ interaction. Phenomenological density functional models seem to favor lower $T_C \sim 10$ MeV, as in the very early work of Sauer *et al.* [1] while values around $T_C \sim 20$ MeV are predicted by microscopic approaches as, for example, in the study of Baldo and Ferreira [3]. Covariant field theory and thermodynamics have been studied very frequently. A comprehensive discussion is found in the early work of Weldon [4]. The connection of a hadron field theory and thermodynamics was discussed by Furnstahl and Serot [5]. Finite temperature many-body theory, the Green functions, and the solution of the G-matrix equation in a transport theoretical connection has been reviewed in detail by Botermans and Malfliet [6]. The same authors have studied intensively in-medium interactions in cold and hot nuclear matter [7, 8]. As reported in [8] they found that the Dirac-Brueckner G-matrix depends only very weakly on temperature. As will be discussed later, this allows to extrapolate interactions safely from the $T = 0$ to the $T > 0$ case. The work of Müller and Serot [9] addresses the thermal properties of asymmetric nuclear matter quite generally. On the basis of a relativistic mean-field model with non-linear self-interactions of the scalar and vector fields and relativistic thermodynamics, the phase structure of nuclear matter with arbitrary proton content was investigated in detail. An unexpected result was that in asymmetric matter instabilities are induced primarily by fluctuations in the proton content rather than by fluctuations in the net baryon density. Hence, *chemical instability* of the composition

of the fluid wins over the *mechanical instability* of the total system, at least in that particular model. The instability region of warm asymmetric nuclear matter has been studied by many other groups. A detailed comparison between relativistic models and Skyrme forces is provided by the work of Dutra et al [10].

The mentioned properties are largely determined by the $NN$-interactions, besides, naturally, Fermi-Dirac statistics. At the energy and momentum scales, relevant for nuclear matter, $NN$-forces are acting like van-der-Waals forces among molecules. Hence, at not too high density, pressure, and temperature nuclear matter resembles a multi-component van-der-Waals gas. However, the exact values of the permissible density and temperature ranges are yet to be determined. It is one purpose of this work to add new aspects to that ongoing research program. As far as temperature is concerned, the QCD-phase transition into a Quark-Gluon-Plasma ($QGP$) at $T_c^{QCD} \sim 150$ MeV is a clear limit. Hence, only temperatures well below $T_c^{QCD}$ should be considered. We choose a temperature range $T < 100$ MeV. The density behavior is much less constraint. The assumed central density of a neutron star may serve as guideline. Taking into account the recently observed neutron star with a mass of twice the solar mass, we may accept a density range below $6\rho_{eq}$, where $\rho_{eq} = 0.16fm^{-3}$ is the density of symmetric nuclear matter density at the saturation point.

In addition to the liquid-gas phase transition, equilibrated nuclear matter may undergo other phase transitions by creating hadrons. Pion and kaon condensation has been investigated theoretically, and also the thermal production of excited baryons like the $\Delta(1232)$ resonance were considered. However, clear experimental signals indicating such hadron condensation with the sudden appearance of a new type of species in the fluid are still missing. Better established are bosonization processes in cold matter at extremely low densities: under such conditions nuclear matter rearranges into bound constituents, forming deuterons and, especially, $\alpha$ particles. In the crust of neutron stars, one expects a lattice of heavier nuclei up to the iron and nickel region [11]. Finite temperature effects on the geometrical formation of the neutron star crust have been analyzed in detail by Gögelein et al. [12]. Here, we consider pure uniform nuclear matter, composed of nucleonic quasi-particles only but with an arbitrary mixture of protons and neutrons. A very complete and comprehensive discussion of thermal dynamics in asymmetric nuclear matter is found in the already cited work by Müller and Serot [9]. These authors have pointed out in remarkable clarity the important differences between the thermodynamics of symmetric and pure neutron matter on the one side and the thermodynamics of asymmetric matter. Symmetric and neutron matter as single component systems with a single conserved charge, namely baryon number, are corresponding to a pure classical van-der-Waals gas. As the latter, symmetric and neutron matter develop first order phase transitions. This is no longer the case for multi-component systems as asymmetric nuclear matter where protons and neutrons occupy in momentum space different Fermi spheres. Within the relativistic mean-field model used in [9] quantal multi-component systems change their state of aggregation by second order phase transitions. Hence, if a phase transition is going to happen in a charge asymmetric nuclear system signals will be washed out, complicating the identification of critical phenomena. Clearly, this is a strict result only for equilibrium thermodynamics based on consideration of infinite matter. Transport-like non-equilibrium conditions as encountered in a heavy ion collision underly their own special dynamical and statistical laws as e.g. in fragmentation reactions [13–15]. Interestingly, as discussed in those papers grand canonical thermodynamics is a successful concept also for fragmentation processes.

The investigations in [9] are based on the non-linear extension of the original Walecka model, allowing for self-interactions of the scalar-isoscalar field. Those approaches are completely phenomenological in nature without attempting to relate the model parameters to an underlying theory. Here, we follow a different approach by using the DDRH nuclear field theory providing an easy to handle and flexible description of equilibrated cold and hot nuclear matter. DDRH theory, developed some time ago in Giessen, [16–20], is a density dependent field theory with interactions derived by Dirac-Brueckner theory from free space $NN$-interactions. The one-boson exchange picture on which DDRH theory is based, gives access to the full spectrum of scalar, pseudo-scalar, and vector interaction channels, typically described in terms of meson-exchange interactions. The medium dependence is taken into account by vertex functionals depending on Lorentz-invariant binomials of the baryon field operators. Their mean-field expectation values are evaluated by relations using the self-consistent scheme of Dirac-Brueckner Hartree-Fock theory. In this sense, the density dependent relativistic hadron (DDRH) field theory is a parameter-free *ab initio* description of nuclear matter. In particular, the microscopic ansatz gives access to details unreachable for phenomenological approaches. One of those regions is the contribution of isovector-scalar interactions as realized in nature by the $a_0(980)$ meson. The importance of the corresponding scalar-isovector mean-field for asymmetric nuclear matter was pointed out in our previous work [19, 20], deriving for the first time the density dependence of the $\delta$-$NN$ vertex by DBHF calculations. Since then, the interaction channel is being included as a standard tool in many nuclear interaction studies, see e.g. [21, 22]. Obviously, this is a short-range phenomenon acting in competition with the vector meson repulsion. However, the consequences are quite different and important: scalar fields modify the relativistic effective masses of baryons. Hence, they change the mechanical properties. Since isovector-scalar fields lead in asymmetric nuclear matter to counterbalanced modifications of proton and neutron effective masses we have to expect important modifications of the dynamical and, especially, the thermodynamical laws. Here, we present for the first time extensions of DDRH

theory to equilibrated nuclear matter at finite temperature. To a large extent, the results obtained in the present work are representative for any type of nuclear field theory based on density dependent meson-baron vertices. However, an essential and unique feature over other work is the inclusion of scalar-isovector interactions. In a relativistic approach the corresponding self-energies are leading to a splitting of the proton and neutron relativistic effective masses in asymmetric matter, thus changing the inertial properties of the particle species in an asymmetric manner. An important built-in property of DDRH theory is the conservation of the Hugenholtz-van Hove (HVH) theorem [23]. Rearrangement self-energies, accounting for the static polarization of the medium, are playing the essential role [17] in conserving the HVH relation. Since thermodynamical consistency is fulfilled at all densities and temperatures, we are avoiding artificial effects from violations of the HVH theorem which will appear inevitably when density dependent effective interactions like a Brueckner G-matrix are used but rearrangement self-energies are neglected.

The nuclear many-body theoretical background is discussed in sect.II, the relevant thermodynamical quantities are introduced in sect.III. In sect. IV we present our results on the EOS in mean-field approximation of symmetric nuclear matter and in sect. V those for asymmetric nuclear matter. We also compare the DDRH results to those obtained from the DD-ME2 model [24], which is a phenomenological derivative of our DDRH theory. In this model the density dependent vertices are fitted directly to nulear data. Typically, DD-ME models neglect the $\delta$ mean-field. Additionally, in order to emphasize the impact of the density dependent formulation on various properties of nuclear matter, the results from the NL3[25], the QHD model model with constant interaction vertices [26] and the non-relativistic Skyrme type model [27] are shown. For this purpose, we use the QHD model with $\sigma$, $\omega$ and $\rho$ mesons in its original formulation [26, 28]. In particular, we discuss the influence of the isovector-scalar self-energies on the binodal and spinodal structures. Conclusions are drawn and an outlook is given to open questions and future work in sect.VI.

## II. DENSITY DEPENDENT HADRON FIELD THEORY

### A. The DDRH Lagrangian and Energy Momentum Tensor

An important step forward in understanding the saturation properties of infinite nuclear matter was achieved by theories describing in-medium interactions microscopically. Using relativistic Dirac-Brueckner (DB) it was found that the pertinent problem of non-relativistic G-matrix calculations, namely by always ending up at the Coester-line and missing the empirical saturation point of infinite nuclear matter, could be overcome. With standard free-space $NN$-interactions, reproducing well the $NN$ scattering observables, the empirical saturation properties of nuclear matter could be described convincingly well [19, 29–34]. Using realistic nucleon-nucleon meson-exchange potentials, in-medium interactions are derived by complete resummation of (two-body) ladder diagrams. Since full-scale DB calculations for finite heavy nuclei are not feasible a practical approach is to derive from infinite matter DB results an equivalent energy density functional. The Kohn-Sham [35] and the Hohenberg-Kohn [36] theorems confirm the existence of a general density functional, although they do not provide a guideline for construction. Based on the work in [33, 37] we have derived in [16, 17] a fully covariant and thermodynamically consistent field theory by treating the interaction vertices as Lorentz-scalar functionals of the nucleonic field operators. The DDRH approach, unlike common relativistic mean field (RMF) models, accounts for quantal fluctuations of the baryon fields even in the ground state. In [18] the DDRH theory has been applied to asymmetric nuclear matter and nuclei far from stability. An appropriate set of coupling constants has been derived, now including isoscalar ($\sigma$,$\omega$) and isovector ($\delta$,$\rho$) vertices. In turn, a phenomenological approach to DDRH theory was proposed by Typel and Wolter [38], trying to derive the density dependence of the vertices empirically by fits to nuclear data. Since then, a large variety of purely phenomenological models has been formulated by several groups and are being applied successfully to nuclei over almost the full mass table.

In the fully microscopic *ab initio* approach of the DDRH theory one considers nuclear systems composed of protons and neutrons, described by Dirac field operators $\Psi_q$ with $q = p, n$. Interactions are derived in the one boson exchange approximation by using a set of mesons, mainly acting as virtual fields and thus providing the interactions among the nucleons. Our relativistic boson exchange model includes pseudoscalar $(\pi, \eta)$, scalar $(\sigma, \delta/a_0(980))$ and vector mesons $(\omega, \rho)$. The Lagrangian is given by

$$\mathcal{L} = \mathcal{L}_N + \mathcal{L}_M + \mathcal{L}_{\rm int}. \tag{2.1}$$

The fermionic part for the matter fields $\Psi_q$ is of standard Dirac-form:

$$\mathcal{L}_N = \sum_{q=p,n} \overline{\Psi}_q \left( i\gamma_\mu \partial^\mu - M_q \right) \Psi_q \quad . \tag{2.2}$$

In the meson sector of the theory we have to distinguish the scalar ($\alpha = \sigma, \delta/a_0(980)$) and pseudoscalar ($\alpha = \eta, \pi$) mesons, obeying equations of the type

$$\mathcal{L}_M^{(\alpha)} = \frac{1}{2}\left(\partial_\mu \varphi_\alpha \partial^\mu \varphi_\alpha - m_\alpha^2 \varphi_\alpha^2\right) \quad . \tag{2.3}$$

The vector mesons ($v = \omega, \rho$) are subject to

$$\mathcal{L}_M^{(v)} = -\frac{1}{2}\left(F_{\mu\nu}^{(v)} F^{(v)\mu\nu} - m_v^2 A_\mu^{(v)} A^{(v)\mu}\right) \quad , \tag{2.4}$$

with the field strength tensors of the vector mesons

$$F_{\mu\nu}^{(\omega)} = \partial_\mu A_\nu^{(\omega)} - \partial_\nu A_\mu^{(\omega)}, \quad \boldsymbol{F}_{\mu\nu}^{(\rho)} = \partial_\mu \boldsymbol{A}_\nu^{(\rho)} - \partial_\nu \boldsymbol{A}_\mu^{(\rho)} - \hat{\Gamma}_\rho(\hat{\rho})\left(\boldsymbol{A}_\mu^{(\rho)} \times \boldsymbol{A}_\nu^{(\rho)}\right), \tag{2.5}$$

where the $\rho$-meson field-tensor includes the non-Abelian isospin term assuming the coupling to the conserved isovector current. Note, however, that the self-interaction term does not contribute in mean field approximation

Of special interest is the interaction part $\mathcal{L}_{\rm int} = \mathcal{L}_{ps} + \mathcal{L}_s + \mathcal{L}_v$ which includes the pseudoscalar vertices

$$\mathcal{L}_{ps} = \hat{\Gamma}_\eta(\hat{\rho})\overline{\Psi}\gamma_5\Psi\varphi_\eta + \frac{f_\eta}{m_\eta}\overline{\Psi}\gamma_5\gamma_\mu\Psi\partial^\mu\varphi_{ps} + \hat{\Gamma}_\pi(\hat{\rho})\overline{\Psi}\gamma_5\boldsymbol{\tau}\Psi\boldsymbol{\varphi}_\pi + \frac{f_\pi}{m_\pi}\overline{\Psi}\gamma_5\gamma_\mu\boldsymbol{\tau}\Psi\partial^\mu\boldsymbol{\varphi}_\pi \tag{2.6}$$

the scalar vertices,

$$\mathcal{L}_s = \hat{\Gamma}_s(\hat{\rho})\overline{\Psi}\Psi\varphi_s + \hat{\Gamma}_\delta(\hat{\rho})\overline{\Psi}\boldsymbol{\tau}\Psi\boldsymbol{\varphi}_\delta \tag{2.7}$$

and the vector meson interactions, respectively,

$$\mathcal{L}_v = \hat{\Gamma}_\omega(\hat{\rho})\left(\overline{\Psi}\gamma_\mu\Psi A^{(\omega)\mu} + \frac{f_\omega}{m_\omega}\overline{\Psi}\sigma_{\mu\nu}\Psi F^{(\omega)\mu\nu}\right) + \hat{\Gamma}_\rho(\hat{\rho})\left(\overline{\Psi}\boldsymbol{\tau}\gamma_\mu\Psi\boldsymbol{A}^{(\rho)\mu} + \frac{f_\rho}{m_\rho}\overline{\Psi}\sigma_{\mu\nu}\boldsymbol{\tau}\Psi\boldsymbol{F}^{(\rho)\mu\nu}\right) \quad . \tag{2.8}$$

A Lagrangian of the same type, but with bare coupling constants $\Gamma_\alpha(\rho) \to g_\alpha = const.$, is used for free space $NN$ scattering, serving to fix the bare coupling constants. The full set of mesons with the respective coupling constants is used to obtain first the free space T-matrix and the in-medium Dirac-Brueckner G-matrix. As discussed in [19] the Driac-Brueckner Hartree Fock calculations are performed in asymmetric nuclear matter, making it possible to derive the full set of isoscalar and isovector self-energies. The self-energies contain via u-channel processes also pion and eta-meson contributions. They are in fact important for a proper description of the density dependence of the self-energies. As discussed in refs. [17–19] the self-energies are used to derive effective density dependent Hartree-vertices. Because, owing to parity pseudo-scalar mesons do not develop classical, condensed fields neither the pion nor the eta-meson fields contribute to the mean-field sector of the theory. They are, however, present in dynamical processes leading to excitations of the system. Here, we are considering nuclear thermodynamics only on the mean-field level, thus leaving investigations of dynamical fluctuations to a future study. Hence, for the present work only the scalar and the vector interaction Lagrangians, Eq. (2.7) and Eq. (2.8), respectively, will be of direct relevance once we have derived the DBHF vertices.

The Lagrangian of Eq. (2.1) is highly non-linear in the fermionic field operators contained in the density operator $\hat{\rho}$. At the theoretical-mathematical level, this is a wanted property because it allows us to keep full control over all changes of the systems and imposes covariance of the field equations. The derivation of the vertex functionals and their explicit determination in mean-field approximation as functions of the density is discussed in [18].

With the standard Legendre-transformation we obtain the DDRH energy momentum tensor $T^{\mu\nu}$ [17, 20]. Of particular interest is the Hamiltonian density

$$\begin{aligned}\mathcal{H} \equiv T^{00} \;=\; & \overline{\Psi}\gamma_0\Sigma^{0(0)}\Psi + \overline{\Psi}\left(M - \Sigma^{s(0)}\right)\Psi + \sum_{\alpha=\sigma,\delta,\pi}\left((\partial^0\phi_\alpha)^2 - \frac{1}{2}\left[\partial_\lambda\phi_\alpha\partial^\lambda\phi_\alpha - m_\alpha^2\phi_\alpha^2\right]\right) \\ & + \sum_{\alpha=\omega,\rho}\left(\partial^0 A_\lambda F^{(\alpha)\lambda 0} - \frac{1}{2}\left[m_\alpha^2 A_\mu^{(\alpha)} A^{\mu(\alpha)} - F_{\lambda\rho}^{(\alpha)} F^{\lambda\rho(\alpha)}\right]\right)\end{aligned} \tag{2.9}$$

The full energy momentum tensor $T^{\mu\nu}$ includes rearrangement contributions induced by the functional derivatives of the vertex functional [16–18], modifying in particular the pressure density $P \sim T^{ii}$.

By the standard techniques of finite temperature quantum many-body theory [39], we introduce hadronic chemical potentials $\mu_q$ and the corresponding number operators $N_q$. Covariant thermodynamics will be discussed below. Here,

we only indicate the connection to the more familiar non-relativistic formulation. This is achieved by a canonical transformation

$$K = H - \sum_{\eta} \mu_{\eta} N_{\eta} \tag{2.10}$$

from which the grand partition function is obtained

$$Z_G = e^{-\beta\Omega} = \mathrm{Tr}\, e^{-\beta K} \tag{2.11}$$

and the statistical operator

$$\rho_G = Z_G^{-1} e^{-\beta\Omega} = e^{-\beta(\Omega - K)} \tag{2.12}$$

is serving to perform the thermodynamical average of observables over the grand canonical ensemble. Explicit expression are derived below.

### B. The DDRH Field Equations and Mean-Field Approximation

From the above Lagrangian we derive by variation with respect to the Dirac-adjoint fermion field operators $\overline{\Psi}$ wave equations of Dirac-type,

$$\left(\gamma_\mu (i\partial^\mu - \Sigma_v^\mu) - M - \Sigma_s\right) \Psi = 0 \quad . \tag{2.13}$$

They include the vector and scalar self-energies $\Sigma_v^\mu$ and $\Sigma_s$, respectively [16]. The variation leads to two distinct types of self-energies,

$$\Sigma = \Sigma^{(b)} + \Sigma^{(r)} \tag{2.14}$$

$$\Sigma^{(b)} = \frac{\partial \mathcal{L}_{int}}{\partial \overline{\Psi}} \tag{2.15}$$

$$\Sigma^{(r)} = \frac{\partial \mathcal{L}_{int}}{\partial \hat{\rho}} \frac{\delta \hat{\rho}}{\delta \overline{\overline{\Psi}}} \tag{2.16}$$

The bare self-energies $\Sigma^{(b)}$ are of the conventional structure as also obtained in a theory with density-independent, constant vertices. Since our vertex functionals are derived from Dirac-Brueckner theory, they correspond to the standard DBHF self-energies [8, 19]. The rearrangement self-energies $\Sigma^{(r)}$ in Eq. (2.16) represent an essential new feature of generic character for a density dependent formalism. It is seen that these contributions originate from the variation of the vertex functionals, thus describing the response of interaction vertex on a change of the medium. Physically, $\Sigma^{(r)}$ accounts for the dynamical rearrangement effects of the nuclear medium by virtue of polarization [16, 20].

The meson field equations are given by the standard Klein-Gordan equations for the scalar and pseudo-scalar fields,

$$\left(\partial_\mu \partial^\mu + m_\alpha^2\right) \Phi_\alpha = \hat{\Gamma}_\alpha(\hat{\rho}) \overline{\Psi} \hat{O}_\alpha \Psi \tag{2.17}$$

where $\hat{O}_\alpha \in \{1, \gamma_\mu, \gamma_5\} \otimes \{1, \tau\}$ and derivative terms may contribute as well. The vector fields obey the Proca-equation

$$\partial_\mu F^{(\alpha)\mu\nu} + m_\alpha^2 A^\nu = \hat{\Gamma}_\alpha(\hat{\rho}) \overline{\Psi} \hat{J}_\alpha^\nu \Psi \tag{2.18}$$

where $\overline{\Psi} \hat{J}_\alpha^\nu \Psi$ denotes the corresponding vector current. The only difference is that the vertices depend now on the background medium. For our purpose, the Bose-fields are far off their mass shell. They are virtual fields which are fully determined by their nucleonic sources, contributing only in $t-$ and $u-$channel processes among nucleons.

The field equations are to be solved for a given nuclear matter ground state configuration. Using the mean.field approximation we specify the expectation values of the functionals. Let $\rho = \langle \hat{\rho} \rangle$ be the ground state expectation value of the operator $\hat{\rho} = \hat{\rho}(\bar{\Psi}_q, \Psi_q)$ which is a Lorentz-scalar functional of the proton and neutron, respectively, field operators $\Psi_q$. Using $\hat{\rho} = \rho + \delta\rho$ we expand the vertex functionals according to

$$\Gamma_\alpha(\rho + \delta\rho) = \Gamma_\alpha(\rho) + \left.\frac{\partial \Gamma_\alpha(\hat{\rho})}{\partial \hat{\rho}}\right|_\rho \delta\rho + \cdots \tag{2.19}$$

Taking the ground state expectation value of the vertex, the first order correction $\delta\rho = \hat{\rho} - \rho$ vanishes identically, The first non-vanishing correction is given by

$$C(\hat{\rho}) = \langle(\hat{\rho} - \rho)^2\rangle = \langle\hat{\rho}\rangle^2 - \rho^2 \quad , \tag{2.20}$$

determined by the quantal fluctuations of $\hat{\rho}$ with respect to the reference value $\rho$. In ground state calculation we neglect terms of this and higher order consistently. Therefore, in nuclear matter the meson field equations are always determined by source terms with a strength given by $\Gamma_\alpha(\rho)$, which is a number given as a function of $\rho$.

Thus, neglecting consistently all non-stationary fluctuations around the ground state expectation values, we obtain the mean-field equations

$$\left(\vec{\nabla}^2 - m_\alpha^2\right)\Phi_\alpha = -\Gamma_\alpha(\rho)\langle\overline{\Psi}\mathcal{O}_{(\alpha)}\psi\rangle \tag{2.21}$$

$$\left(\vec{\nabla}^2 - m_\alpha^2\right)A^{(\alpha)\mu} = \Gamma_\alpha(\rho)\langle\overline{\Psi}\mathcal{O}^{(\alpha)\mu}\psi\rangle \quad , \tag{2.22}$$

where the fields are now classical scalar and vector fields, respectively.

In the following we will apply the mean-field approximation to the full Lagrangian, Eq. (2.1). As a consequence of time reversal invariance and parity conservation, the pseudo-scalar and pseudo-vector fields will become identical to zero in the ground state. However, there is still an implicit contribution of these fields to the of the remaining density dependent couplings, since they are derived from the full Dirac-Brueckner theory. This can be seen with the help of the Fierz transformation and decomposition of the exchange diagrams in terms of direct channels. [19]

As already indicated in the previous section, we will use the DDRH theory in mean field approximation, with the explicit inclusion of the $\sigma$, $\delta$, $\omega$ and $\rho$ meson mean-fields. The interaction part of the Lagrangian then simplifies to

$$\mathcal{L}_{\rm int} = \Gamma_\sigma(\rho)\bar{\psi}\Phi_\sigma\psi + \Gamma_\delta(\rho)\bar{\psi}\boldsymbol{\tau}\boldsymbol{\Phi}_\delta\psi - \Gamma_\omega(\rho)\bar{\psi}\gamma_\mu A^{(\omega)\mu}\psi - \Gamma_\rho(\rho)\bar{\psi}\gamma_\mu\boldsymbol{\tau}\boldsymbol{A}^{(\rho)\mu}. \tag{2.23}$$

The first derivative terms in Eq. (2.19) lead to the mean-field rearrangement self-energies, including scalar and vector components:

$$\Sigma^{s(r)} = \sum_\alpha \left(\frac{\partial\Gamma_\alpha}{\partial\hat{\rho}}\Big|_\rho \langle\overline{\Psi}\mathcal{O}_\alpha\psi\rangle\Phi_\alpha\right) \tag{2.24}$$

$$\Sigma^{v(r)} = \sum_\alpha \left(\frac{\partial\Gamma_\alpha}{\partial\hat{\rho}}\Big|_\rho \langle\overline{\Psi}\mathcal{O}_\mu^{(\alpha)}\psi\rangle A^{(\alpha)\mu}\right) \quad . \tag{2.25}$$

The self-energies are decomposed into isoscalar and isovector parts:

$$\begin{aligned}\hat{\Sigma}^{s(0)} &= \hat{\Gamma}_\sigma(\hat{\rho})\phi_\sigma + \hat{\Gamma}_\delta(\hat{\rho})\boldsymbol{\tau}\cdot\boldsymbol{\Phi}_\delta \\ &= \hat{\Sigma}_0^{s(0)} + \boldsymbol{\tau}\hat{\boldsymbol{\Sigma}}_1^{s(0)}\end{aligned} \tag{2.26}$$

and correspondingly, for the vector self-energies

$$\begin{aligned}\hat{\Sigma}^{\mu(0)} &= \hat{\Gamma}(\hat{\rho})A^{(\omega)\mu} + \hat{\Gamma}_\rho(\hat{\rho})\boldsymbol{\tau}\cdot\boldsymbol{A}^{(\rho)\mu} \\ &= \hat{\Sigma}_0^{(0)\mu} + \boldsymbol{\tau}\hat{\boldsymbol{\Sigma}}_1^{(0)\mu}.\end{aligned} \tag{2.27}$$

where we have left out the photon field. For infinite nuclear matter we find explicitly in Hartree approximation [18] the non-vanishing self-energies

$$\begin{aligned}\Sigma_q^{s(0)}(\hat{\rho}) &= \Gamma_\sigma(\hat{\rho})\Phi_\sigma + \tau_q\Gamma_\delta(\hat{\rho})\Phi_\delta \\ \Sigma_q^{0(0)}(\hat{\rho}) &= \Gamma_\omega(\rho)A_0^{(\omega)} + \tau_q\Gamma_\rho(\hat{\rho})A_0^{(\rho)} \\ \Sigma^{0(r)}(\hat{\rho}) &= \frac{\partial\Gamma_\omega}{\partial\hat{\rho}}A_0^{(\omega)}\rho_0 + \frac{\partial\Gamma_\rho}{\partial\hat{\rho}}A_0^{(\rho)}\rho_1 - \frac{\partial\Gamma_\sigma}{\partial\hat{\rho}}\Phi_\sigma\rho^s - \frac{\partial\Gamma_\delta}{\partial\hat{\rho}}\Phi_\delta\rho_1^s \quad ,\end{aligned} \tag{2.28}$$

where proton ($q = p$) and neutron ($q = n$) contributions are indicated and $\tau_q = \pm 1$ denotes the corresponding expectation values of the isospin $\tau_3$ operator, respectively. All vertex derivatives are to be evaluated at $\hat{\rho} = \rho$. Since isospin symmetry requires that the vertices must depend only on isoscalar quantities the rearrangement self-energies do not depend on the nucleonic charge state. Defining the proton and neutron vector densities by $\rho_q = \langle 0|\overline{\Psi}_q\gamma_0\Psi_q|0\rangle$

and similarly the corresponding scalar densities by $\rho_q^s = \langle 0|\overline{\Psi}_q\Psi_q|0\rangle$ we find the isoscalar ($I = 0$) and isovector ($I = 1$) vector and scalar densities, respectively,

$$\rho_I = \rho_n + (-)^I \rho_p \tag{2.29}$$
$$\rho_I^s = \rho_n^s + (-)^I \rho_p \quad . \tag{2.30}$$

It can be easily verified that in Eq. (2.28) the isovector pieces are in fact of quadratic order in $\rho_1$ and $\rho_1^s$, respectively.

The proton and neutron wave functions, respectively, obey Dirac equations of standard form

$$\left[\gamma_\mu\left(i\partial^\mu - \hat{\Sigma}_q^\mu\right) - \left(M_q - \hat{\Sigma}_q^s\right)\right]\Psi_q = 0, \tag{2.31}$$

but with the self-energies as defined as in Eq. (2.14) and constructed by means of the results in Eq. (2.28).

Since we include interactions in the scalar-isovector channel represented by the $\delta/a_0(980)$ meson the effective mass of the nucleons is explicitly isospin dependent in DDRH theory [18, 19],

$$M_q^* = M - \Gamma(\rho)\phi_\sigma - \tau_q\Gamma_\delta(\rho)\phi_\delta. \tag{2.32}$$

## III. THERMODYNAMICS OF NUCLEAR MATTER

### A. Covariant Thermodynamics

In the covariant formulation of thermodynamics it is expedient to express all equations in terms of Lorentz scalars and Lorentz four-vectors. For this purpose we follow the steps from [5] by introducing the thermal potential $\alpha = \beta\mu$ and the thermal time-like four vector $\beta_\mu = \beta u^\mu$, where $u^\mu = \frac{1}{\sqrt{1-v^2/c^2}}(1, \boldsymbol{v})$ is the fluid velocity four-vector and $\beta = 1/T$ the inverse temperature.

A system of a set of conserved currents $j_c^\mu$ in equilibrium is described by the energy momentum tensor $T^{\mu\nu}$ and the entropy flux $\sigma^\mu$. These quantities are connected by the first law of thermodynamics [28, 40]

$$\beta_\nu \mathrm{d}T^{\nu\mu} = \mathrm{d}\sigma^\mu + \sum_c \alpha_c \mathrm{d}j_c^\mu. \tag{3.1}$$

The pressure $P$ can be expressed in terms of the primary functions by

$$P\beta^\mu = -\beta_\nu T^{\nu\mu} + \sigma^\mu + \sum_c \alpha_c j_c^\mu. \tag{3.2}$$

In statistical quantum mechanics the thermodynamic functions are related to ensemble averages of quantum-mechanical operators. This is usually achieved by defining a grand partition function $Z$ and a corresponding four-vector potential $\Phi^\mu(\alpha_c, \beta_\nu)$. The partition function is

$$Z \equiv \mathrm{Tr}\left[\exp\left(\int \mathrm{d}\mathcal{F}_\mu\left[\sum_c \alpha_c j_c^\mu - \beta_\nu T^{\nu\mu}\right]\right)\right] \tag{3.3}$$

where $\mathcal{F}_\mu$ denotes the four-dimensional infinitesimal surface element. By varying $\beta_\nu$ and $\alpha_c$ one can derive a differential equation, that connects $\Phi^\mu$ with the energy momentum tensor and the conserved currents,

$$\mathrm{d}\Phi^\mu = T^{\mu\nu}\mathrm{d}\beta_\nu - \sum_c j_c^\mu \mathrm{d}\alpha_c, \tag{3.4}$$

providing the covariant thermodynamic laws

$$T^{\mu\nu} = \left(\frac{\partial\Phi^\mu}{\partial\beta_\nu}\right)_{\alpha_c}, \tag{3.5a}$$
$$j_{c'}^\mu = -\left(\frac{\partial\Phi^\mu}{\partial\alpha_{c'}}\right)_{\beta_\mu, \alpha_c, c\neq c'}. \tag{3.5b}$$

Furthermore, after differentiating Eq. (3.2) and using the first law of thermodynamics, Eq. (3.1), we arrive at the covariant form of the Gibbs relation:

$$\Phi^\mu = -P\beta^\mu = \beta_\nu T^{\nu\mu} - \sigma^\mu - \sum_c \alpha_c j_c^\mu \tag{3.6}$$

In the comoving frame $u^\mu = (1,0,0,0)$, thus, Eq. (3.3) reduces to

$$Z \equiv \sum_n \langle n|e^{-\beta(\hat{H}-\sum_c \mu\hat{N}_c)}|n\rangle = \mathrm{Tr}\; e^{-\beta(\hat{H}-\sum_c \mu_c\hat{N}_c)}, \tag{3.7}$$

where $\hat{H}$ is the Hamiltonian describing the system and $\hat{N}_c$ the number operator. In Eq. (3.7) the trace has to be taken as a sum over all energy and particle eigenstates $|n\rangle$. With this, the above expressions lead to a connection between the thermodynamic potential and other thermodynamic functionals:

$$\Phi^\mu(\alpha_c,\beta_\nu) = -\frac{1}{V}\ln Z u^\mu = \frac{\Omega(T,\mu,V)}{TV}u^\mu \tag{3.8a}$$

$$\rho_c = -\frac{1}{V}\frac{\partial\Omega}{\partial\mu_c} \tag{3.8b}$$

$$\mathcal{S} = \beta\left(\mathcal{E} - \Omega - \sum_b \mu_b\rho_b\right) \tag{3.8c}$$

According to the Hugenholtz-Van Hove theorem [23], the thermodynamic and the hydrostatic pressure must coincide, i.e.

$$P = \rho^2\frac{\partial\mathcal{F}}{\partial\rho} = \frac{1}{3}\sum_{i=1}^{3}\langle T^{ii}\rangle, \tag{3.9}$$

with the free energy $\mathcal{F} = \mathcal{E}/\rho - T\mathcal{S}$. In Eq. (3.9) the thermal average is used, which for an arbitrary operator $\hat{O}$ is given by the prescription:

$$\langle\hat{O}\rangle = \frac{\mathrm{Tr}\left[e^{\beta(\hat{H}-\sum_c \mu_c\hat{N}_c)}\hat{O}\right]}{\mathrm{Tr}\left[e^{\beta(\hat{H}-\sum_c \mu_c\hat{N}_c)}\right]} = \mathrm{Tr}\left[\hat{\rho}\hat{O}\right]. \tag{3.10}$$

Consider now the DDRH Hamilton operator, which in mean field approximation (MFA) is given by

$$\begin{aligned}\hat{H}(\hat{\rho}) = T^{00} = \Big[\sum_b\; \bar{\psi}_b\left(i\boldsymbol{\gamma}\boldsymbol{\nabla} + \gamma_0\Sigma_b^{0(0)}(\hat{\rho}) + \left(M - \Sigma_b^S(\hat{\rho})\right)\right)\psi_b \\ + \frac{1}{2}m_\sigma^2\phi_\sigma^2 + \frac{1}{2}m_\delta^2\phi_\delta^2 - \frac{1}{2}m_\omega^2 {A_0^{(\omega)}}^2 - \frac{1}{2}m_\rho^2 {A_0^{(\rho)}}^2\Big],\end{aligned} \tag{3.11}$$

where the sum over $b$ includes all baryons considered in the model. An important consequence of the MFA is the cancellation of the rearrangement term in the Hamiltonian. However, since the interaction vertices are functionals of the density operator $\hat{\rho}$ the calculation of the partition function (3.7) needs to be examined carefully. To derive $Z$ it is necessary to evaluate a trace over the eigenstates in Fock space. This is only possible if the exponential function can be decomposed into a sum of independent terms. To fulfill this requirement in the DDRH model, the Hamiltonian should be approximated by a one-body operator. For this purpose the density-dependent interaction vertices $\hat{\Gamma}_{b\alpha}$ are expanded around the thermal equilibrium density mean value $\rho_0 = \langle\hat{\rho}\rangle$, keeping only terms up to the first order in $(\hat{\rho} - \rho_0)$ (see also Eq. (2.19))

$$\Gamma_\alpha(\hat{\rho}) = \Gamma_\alpha(\rho_0) + \left.\frac{\partial\Gamma_\alpha}{\partial\hat{\rho}}\right|_{\hat{\rho}=\rho_0}(\hat{\rho}-\rho_0) + \mathcal{O}\left((\hat{\rho}-\rho_0)^2\right).$$

With this assumption the expectation values of the vertex functionals become functions of the density, i.e. $\langle\hat{\Gamma}(\hat{\rho})\rangle \to \Gamma(\rho_0)$. Hence, the Hartree-vertices are now implicitly temperature dependent, $\Gamma(\rho,T) = \Gamma(\rho(T))$. On the other hand this approach implies an expansion for the Hamilton operator

$$H(\hat{\rho}) = H^0(\rho_0) + H^R(\hat{\rho})$$

with

$$H^R(\hat{\rho}) = \Sigma^{(r)}(\rho_0)\,(\hat{\rho}-\rho_0) = \sum_b \left( \left.\frac{\partial \Gamma_{b\sigma}}{\partial \hat{\rho}}\right|_{\hat{\rho}=\rho_0} \phi_\sigma \rho_b^s + \left.\frac{\partial \Gamma_{b\delta}}{\partial \hat{\rho}}\right|_{\hat{\rho}=\rho_0} \phi_\delta \tau_b^3 \rho_b^s \right.$$
$$\left. + \left.\frac{\partial \Gamma_{b\omega}}{\partial \hat{\rho}}\right|_{\hat{\rho}=\rho_0} A_\omega^0 \rho_b + \left.\frac{\partial \Gamma_{b\rho}}{\partial \hat{\rho}}\right|_{\hat{\rho}=\rho_0} A_\rho^0 \tau_b^3 \rho_b \right) (\hat{\rho}-\rho_0) \tag{3.12}$$

This shows that the in-medium correlations described by the density-dependent couplings indeed are inducing a rearrangement perturbation in the Hamilton operator. Given this approximation, all operators in the exponential of the partition function are now diagonal. This makes an exact calculation feasible. From the stationary solution of the Dirac equation in MFA we find the energies for baryons and anti-baryons at the equilibrium nuclear matter density $\rho_0$

$$\varepsilon_b^{\pm}(k) = \pm E_b^*(k) + \Sigma_b^{0(0)} + \Sigma^{(r)}(\rho_0), \tag{3.13}$$

with $E_b^*(k) = \sqrt{k^2 + M_b^{*2}}$. Considering the normal ordered products of the baryon fields we can now go through the usual steps for the calculation of the partition function. Indeed, introducing effective baryon masses and effective chemical potentials as

$$M_b^* \equiv M_b - \Sigma_b^S$$
$$\nu_b \equiv \mu - \Sigma_b^0 = \mu - \Sigma_b^{0(0)} - \Sigma^{(r)}, \tag{3.14}$$

leads to the same expression for the baryonic part of the thermodynamic potential as in the non-interacting case. This time, however, the baryon masses and the chemical potentials are replaced by their effective values. Since the meson fields are treated as classical fields their contribution to the partition function is trivial. Thus we can split $\Phi^\mu$ in a baryon, mean field and rearrangement part

$$\Phi^\mu = \sum_b \Phi_b^\mu + \Phi_{\mathrm{MF}}^\mu + \Phi_{\mathrm{R}}^\mu \tag{3.15}$$

with

$$\Phi_b^\mu = -\sum_s \int \frac{\mathrm{d}^3k}{(2\pi)^3} \left[ \ln\left(1 + e^{-\beta(E_k^* - \nu_b)}\right) + \ln\left(1 + e^{-\beta(E_k^* + \nu_b)}\right) \right] u^\mu \tag{3.16}$$

$$\Phi_{\mathrm{MF}}^\mu = \beta \left( \frac{1}{2} m_\sigma^2 \phi_\sigma^2 + \frac{1}{2} m_\delta^2 \phi_\delta^2 - \frac{1}{2} m_\omega^2 {A_0^{(\omega)}}^2 - \frac{1}{2} m_\rho^2 {A_0^{(\rho)}}^2 \right) u^\mu \tag{3.17}$$

$$\Phi_R^\mu = -\beta \rho_0 \Sigma_0^{(r)} u^\mu. \tag{3.18}$$

The fluctuations around the equilibrium density coming from density dependent correlations show up as rearrangement terms in $\Phi_{\mathrm{R}}^\mu$. Consequently, the pressure $P = -\Phi^0/\beta^0$ is also modified by additional rearrangement contributions, which are crucial to fulfill the Hugenholtz-Van Hove theorem. However, the rearrangement parts cancel out in the entropy and energy density. For the latter for example this can be verified by applying Eq. (3.5a) to $\Phi^\mu$,

$$\mathcal{E} = \left.\frac{\partial \Phi^0}{\partial \beta^0}\right|_{\alpha_b} = \sum_b \left( 2 \int \frac{\mathrm{d}^3k}{(2\pi)^3} E_k^* \left( f_B(\nu_b) + \bar{f}_b(\nu_b) \right) + \Sigma_b^{0(0)} \rho_b \right) + \frac{1}{2} \left( \sum_{s=\sigma,\delta} m_s^2 \Phi_s^2 - \sum_{v=\omega,\rho} m_v^2 A_0^{v2} \right) \tag{3.19}$$

Note, that in the calculation of the above derivative all parameters $\alpha_b = \beta\mu_b$ have to be held fixed.

In thermal equilibrium the meson fields should be chosen such that they minimize $\Phi^\mu$, i.e. $\left(\frac{\partial \Omega}{\partial \chi}\right)_{\beta,\mu_b} = 0$ for

$\chi \in \{\phi_\sigma, \phi_\delta, A_0^\omega, A_0^\rho\}$. This results in the following equations

$$\phi_\sigma = \sum_b \frac{\Gamma_{b\sigma}}{m_\sigma^2}\ \rho_b^s \quad \equiv \sum_b \frac{\Gamma_{b\sigma}}{m_\sigma^2} \quad \cdot 2\int\frac{\mathrm{d}^3k}{(2\pi)^3}\ \frac{M_b^*}{E_b^*}\left(f_B(\nu_b,T)+\bar{f}_B(\nu_b,T)\right) \tag{3.20a}$$

$$\phi_\delta = \sum_b \frac{\Gamma_{b\delta}}{m_\delta^2}\ \rho_b^{s(3)} \equiv \sum_b \frac{\Gamma_{b\delta}}{m_\delta^2}\cdot 2\tau_b^3\int\frac{\mathrm{d}^3k}{(2\pi)^3}\ \frac{M_b^*}{E_b^*}\left(f_b(\nu_B,T)+\bar{f}_B(\nu_b,T)\right) \tag{3.20b}$$

$$A_0^\omega = \sum_b \frac{\Gamma_{b\omega}}{m_\omega^2}\ \rho_b \quad \equiv \sum_b \frac{\Gamma_{b\omega}}{m_\omega^2} \quad \cdot 2\int\frac{\mathrm{d}^3k}{(2\pi)^3}\ \left(f_B(\nu_b,T)-\bar{f}_B(\nu_b,T)\right) \tag{3.20c}$$

$$A_0^\rho = \sum_b \frac{\Gamma_{b\rho}}{m_\rho^2}\ \rho_b^3 \quad \equiv \sum_b \frac{\Gamma_{b\rho}}{m_\rho^2}\cdot 2\tau_b^3\int\frac{\mathrm{d}^3k}{(2\pi)^3}\ \left(f_B(\nu_b,T)-\bar{f}_B(\nu_b,T)\right) \tag{3.20d}$$

In the limit of $T \to 0$ the particle distribution function becomes the well known step function, $f_B(\nu_B) \to \Theta\left(\nu_b - E_k^*\right) \equiv \Theta(k_{F_b} - k)$, while the anti-particle distribution function $\bar{f}_B$ vanishes completely. This defines the Fermi momenta and Fermi energies of the baryons as $\nu_b = E_{F_b}^* = \sqrt{k_{F_b}^2 + M_b^{*2}}$. The solution of the baryon densities and, accordingly, the vector meson fields becomes trivial for vanishing $T$, while the scalar densities can be found by a self-consistent solution of the transcendental equation

$$\rho_b^s = \frac{M_b^*}{2\pi^2}\left(E_{F_b}^* k_{F_b} - M_{F_b}^{*2}\ln\left[\frac{E_{F_b}^* + k_{F_b}}{M_b^*}\right]\right) \tag{3.21}$$

The energy density and pressure of cold nuclear matter are then given by:

$$\mathcal{E}(T=0) = \sum_b \frac{1}{4}\left(3E_{F_b}\rho_b + M_b^*\rho_b^s\right) + \sum_b \frac{1}{2}\left(\rho_b\Sigma^{0(0)_b} + \rho_b^s\Sigma_b^S\right) \tag{3.22}$$

$$P(T=0) = \frac{1}{4}\sum_b \left(E_{F_b}\rho_b - M_b^*\rho_b^s\right) + \frac{1}{2}\sum_b\left(\rho_b\Sigma_b^{0(0)} - \rho_b^s\Sigma_b^S\right) + \rho\Sigma^{(r)}, \tag{3.23}$$

where $\rho = \sum_b \rho_b$ is the total baryon density.

### B. The Density and Temperature Dependence of DDRH Vertices and Self-Energies

Typically, nuclear matter mean-field models assume tacitly that interactions are essentially unaffected by temperature. Already quite early, ter Haar and Malfliet [8] have addressed that question by means of finite temperature DBHF calculations. They indeed find a weak temperature dependence of the resulting G-matrix interaction. A closer inspection of the DB-equations at $T > 0$ reveals the reason for that behavior.

The medium and temperature dependence of the G-matrix is introduced by two sources, namely the Pauli blocking of the Fermi-sphere of occupied single particle states and the baryon self-energies. In leading order contributions from the Pauli principle, i.e. Fermi-statistics, are dominant. Therefore, preparatory to the discussion of the equation of state, we should take a closer look at the DDRH vertices first. In Fig. 1 the density-dependence of the DDRH vertices is shown. One can nicely see that the density-dependence has its most impact in the lower density region, and becomes less significant for $\rho > 0.5\mathrm{fm}^{-3}$. Basically, this circumstance arises from the fact that in the high density region the contributions from intrinsic particle fluctuations are small compared to the ones coming from the occupied Fermi sea states. The functional behavior of the $\delta$-meson vertex differs considerably from the one of the other mesons. While all other vertices constantly fall off with rising $\rho$ the $\delta$-meson vertex shows a special functional behavior with a minimum at $\rho \approx 0.14\ \mathrm{fm}^{-3}$. The inclusion of this channel is a key feature of the DDRH model, which leads to a splitting of the effective nucleon masses in asymmetric nuclear matter, as will be are later. The DDRH vertices are deduced from comparing the DDRH potential energy with the Brueckner calculations [17, 18]. In general, the proper DB self-energies, $\Sigma^{\mathrm{DB}}$, are momentum dependent, while the DDRH self-energies are not, since they are calculated in the mean-field approximation. The usual approach to map $\Sigma^{\mathrm{DDRH}}(\rho,T)$ on $\Sigma^{\mathrm{DB}}(k,\rho,T)$, is to calculate the average of $\Sigma^{\mathrm{DB}}$ over the Fermi sea. For the vector self-energies this implies

$$\Sigma_\alpha^{\mathrm{DDRH}}(\rho,T) = \rho\frac{\Gamma_\alpha^2}{m_\alpha^2} = \frac{4}{(2\pi)^3}\frac{1}{\rho}\int \mathrm{d}^3k\ \Sigma_\alpha^{\mathrm{DB}}(k,\rho,T)\left(f_B - \bar{f}_B\right). \tag{3.24}$$

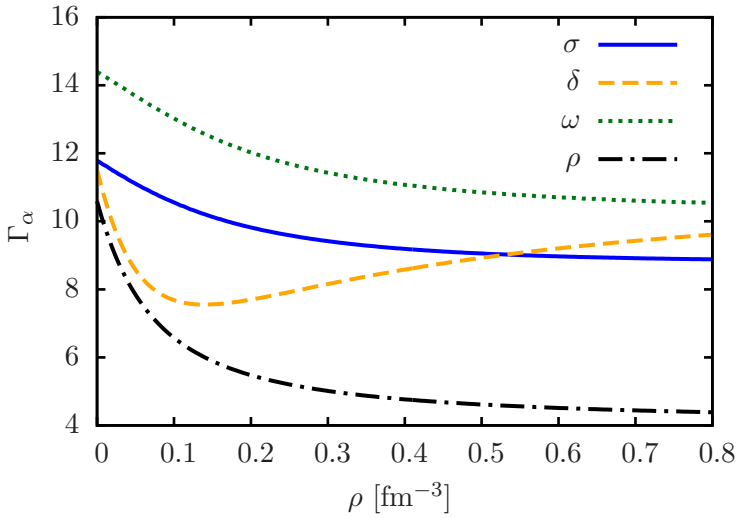


Figure 1: (Color online) Density dependence of the DDRH nucleon-meson vertices at $T = 0$ [18].

For scalar self-energies $\rho$ has to be replaced by $\rho_s$ on the left hand side of (3.24).
In [19] it was shown that the DB self-energies can be approximated by quadratic functions in the momentum $k$ in the vicinity of the Fermi momentum $k_F$. Hence, an expansion of $\Sigma^{\mathrm{DB}}$ up to the first order in $k^2$ around the Fermi momentum is necessary and sufficient to reproduce the DB equation of state properly,

$$\Sigma^{\mathrm{DB}}(k,\rho) \approx \Sigma_F^{\mathrm{DB}}(\rho) + \left(k^2 - k_F^2\right) \Sigma_F'^{\mathrm{DB}}(\rho), \tag{3.25}$$

with the definitions: $\Sigma_F^{\mathrm{DB}} = \Sigma^{\mathrm{DB}}(k_F,\rho)$, $\Sigma_F'^{\mathrm{DB}} = \left.\frac{\partial \Sigma^{\mathrm{DB}}(k,\rho)}{\partial k}\right|_{k=k_F}$.
The Fermi momentum $k_F$ is given by the relation $\sqrt{k_F^2 + M^{*2}} = \nu$ at $T = 0$. Thus, $k_F$ is not well defined for $T > 0$ and should be replaced by a more suitable quantity at finite $T$. One possibility is to define the momentum $k_S$, where the Fermi distribution is half its value at $k = 0$,

$$f_B\left(k_S, T, \nu\right) = \frac{1}{2} f_B\left(0, T, \nu\right)$$

Since the weight-factor $k^2 f_B(k,T,\nu)$ in the momentum integral peaks near $k_S$, it is useful to evaluate $\Sigma^{\mathrm{DB}}$ around this momentum value instead. Because $k_S \to k_F$ for $T \to 0$, this definition is compatible to zero temperature calculations. In Fig. 2 $k_S$ is plotted as a function of $\rho$ for some temperature values. One can see that there is only a significant difference at low densities and high temperatures between $k_S$ and $k_F$. The differences between $\Sigma^{\mathrm{DB}}(k_S)$ and $\Sigma^{\mathrm{DB}}(k_F)$ are very small in this region. This was also found by ter Haar and Malfliet in [7]. Nevertheless, we will substitute $k_F$ by $k_S$ in (3.25) from now on to provide a well defined expansion scheme for all temperatures. In the range of moderate temperatures the DB self-energies show a very small temperature dependence [7, 41]. As an example, Fig. 3 illustrates the temperature dependence of $\Sigma^{\mathrm{DB}}$ as obtained by [7]. From this we conclude, that it is not only possible to apply the same quadratic expansion of $\Sigma^{\mathrm{DB}}$ as suggested by [19] at $T > 0$, but even to neglect the temperature dependence of the self-energies in a first order approximation. Substituting $\Sigma^{\mathrm{DB}}$ by (3.25) in (3.24) gives the following expression for the momentum corrected DDRH vertices:

$$\begin{aligned}\Gamma_\alpha^2 &= \frac{4m_\alpha^2}{(2\pi)^3}\frac{1}{\rho_\alpha}\Sigma_S\left(1 + \frac{\Sigma_S'}{\Sigma_S}\cdot\frac{1}{\rho}\int \mathrm{d}^3k \left(k^2 - k_S^2\right)\left(f_B - \bar{f}_B\right)\right) \\ &\equiv \Gamma_{(0)\alpha}^2\left(1 + C_S^\alpha I_M\right)\end{aligned} \tag{3.26}$$

In (3.26) $\rho_\alpha$ corresponds to $\rho$ and $\rho_s$ for vector and scalar mesons, respectively. $\Gamma_{(0)\alpha}$ is the first order approximation to the dressed vertex, including only Hartree contributions from DB self-energies. For vector mesons $\Gamma_{(0)\alpha}$ is density dependent, while for scalar mesons it additionally depends on the temperature, since $\rho_s$ is a function of $T$ at fixed $\rho$.

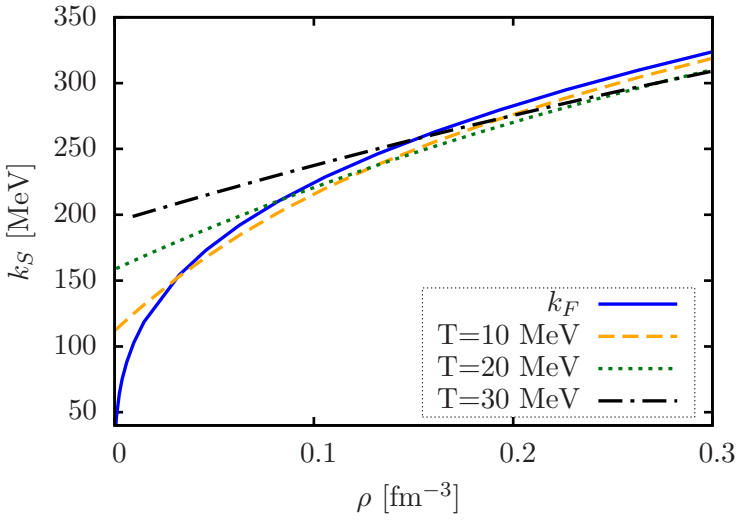


Figure 2: (Color online) Comparison of $k_S$ versus the Fermi momentum $k_F$ for $T$=10, 20 and 30 MeV.

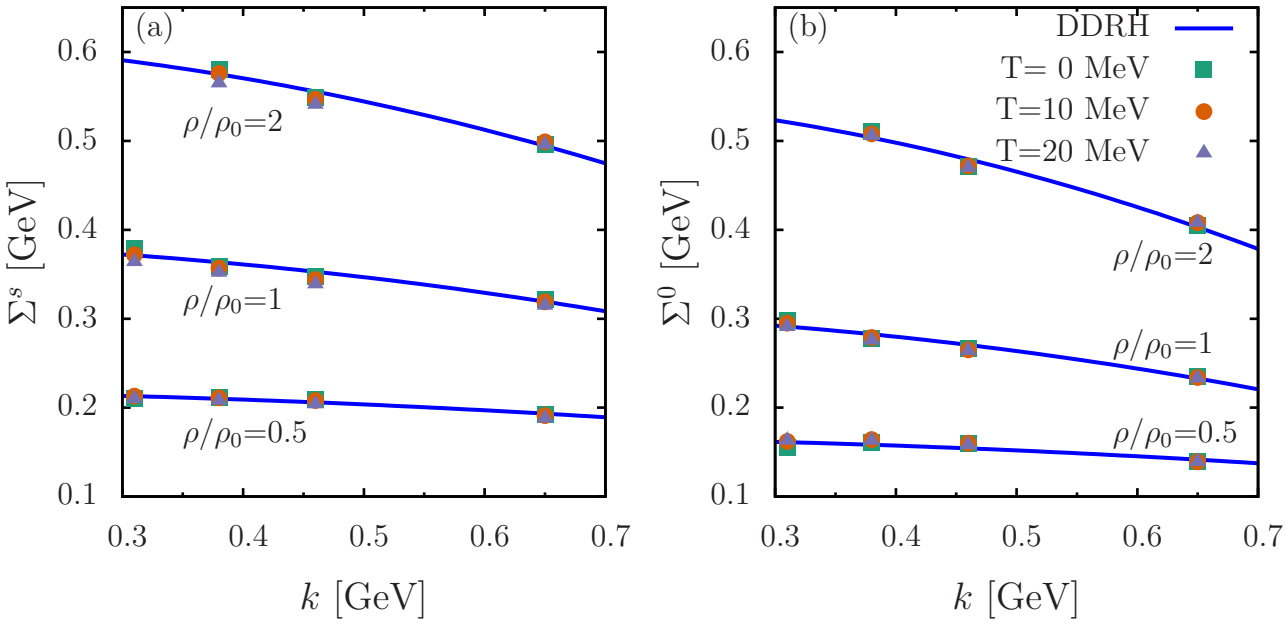


Figure 3: (Color online) The real part of the scalar, (a), and vector, (b), Dirac-Brueckner self-energies at different temperatures and densities, [8], compared to the quadratic approximation discussed in the text.

In this case we can further separate $\Gamma_{(0)s}$

$$\Gamma_{(0)s}(\rho,T)=\tilde{\Gamma}_{(0)s}(\rho)\cdot\sqrt{\frac{\rho_s(T=0)}{\rho_s(T)}}\equiv\tilde{\Gamma}_{(0)s}(\rho)\cdot I_s(\rho,T) \tag{3.27}$$

Obviously, $\Gamma_{(0)s}(T=0)=\tilde{\Gamma}_{(0)s}$. The function $I_s$ provides an additional temperature correction to the scalar vertex. It is important to note here, that a modification of $\Gamma_s$ causes a modification of $\rho_s$, which in turn implies a different value for $\Gamma_s$. Therefore, $I_s(\rho,T)$ must be calculated numerically by solving the self-consistency problem.

The second term in (3.26) incorporates momentum corrections to the vertex, where $C_S^\alpha = \Sigma_S^{\alpha'}/\Sigma_S^\alpha$ and the momentum integral $I_M$ is given by

$$I_M(\rho,T) = \frac{2}{\pi^2\rho}\int \mathrm{d}k\; k^2\left(k^2 - k_S^2(T)\right)\left(f_B(T) - \bar{f}_B(T)\right).$$

As already mentioned, the parameter $C_S$ can be assumed as independent of density and temperature. However, the momentum integral depends explicitly on both, $\rho$ and $T$,

$$I_M = I_M(\rho,T)$$

At $T = 0$ the expression for $\Gamma_\alpha^2$ simplifies to

$$\Gamma_\alpha^2(\rho,T=0) = \tilde{\Gamma}_{(0)\alpha}^2\left[1 + C_S^\alpha\frac{2}{\pi^2\rho}\left(-\frac{2}{15}k_F^5\right)\right] = \tilde{\Gamma}_{(0)\alpha}^2\left[1 - \frac{2}{5}C_S^\alpha k_F^2\right] = \tilde{\Gamma}_{(0)\alpha}^2\left[1 - \kappa C_S^\alpha\rho^{2/3}\right], \tag{3.28}$$

with $\kappa = \frac{2}{5}(\frac{3}{2}\,\pi^2)^{\frac{2}{3}}$.
As thermal excitations become important with increasing $T$, the momentum correction integral $I_M$ will considerably differ from $\kappa\rho^{\frac{2}{3}}$. The constant factor $\kappa C_S^\alpha$ however turns out to be very small leading to a modification of the scalar and vector couplings by only 0.8% and 0.1%, respectively [18]. Therefore, the temperature dependence of $\Gamma_\alpha$ induced by $I_M$ remains small in the temperature and density ranges relevant for this work. For further discussion, we introduce the function $I_C^\alpha$,

$$I_C^\alpha(\rho,T) \equiv \left[\frac{(1 + C_S^\alpha I_M(T))}{(1 + C_S^\alpha I_M(T{=}0))}\right]^{\frac{1}{2}}, \tag{3.29}$$

which describes the temperature dependent correction factor on $\Gamma_\alpha$ arising from the momentum correction integral. This gives the following separation ansatz for $\Gamma_\alpha$:

$$\Gamma^\alpha = \Gamma^\alpha(T{=}0)\cdot I_C^\alpha(T) I_s^\alpha(T). \tag{3.30}$$

Note, that $I_s = 1$ for vector mesons.

In Fig. 4 the functions $I_C^\sigma(T)$ and $I_s^\sigma(T)$ for the $\sigma$-meson coupling are shown at various densities $\rho$. First of all we see, that the temperature dependence becomes less significant with increasing $\rho$. As expected, the momentum correction integral results in small deviations of $\Gamma_\sigma$ from its zero temperature value. While $I_C^\sigma$ falls off continuously with rising $T$ the scalar correction function $I_s^\sigma$ shows an opposite behavior. Thus, the two effects partially compensate each other. In the range of moderate temperatures, where the liquid-gas phase transition takes place, the net correction is less than 0.5% and it stays small even at higher $T$. For the vector coupling $\Gamma_\omega$ we find that the corrections are even less then 0.2%.

This analysis therefore shows, that the approximation

$$\Gamma^{\mathrm{DDRH}}(\rho,T) \approx \Gamma^{\mathrm{DDRH}}(\rho,T=0) \tag{3.31}$$

can be applied for the DDRH vertices. The temperature dependent corrections would have nearly negligible small effects on the finite temperature equation of state for temperatures below 100 MeV. Besides, there are only few experimental data available for warm nuclear matter and it comes with large uncertainties as in the case of liquid-gas critical temperature, for example [42]. Hence, we will use the effective vertices in first order approximation, assuming a density dependence only. Within this approximation our calculations are in very good agreement with other models, as will be shown below. The temperature dependent momentum corrections can be used in future calculations to fine-tune the equation of state properties, whenever more precise data will be available.

In the temperature range considered here, $T < 100$ MeV, the Fermi-Dirac statistics is exerting only little or, at best, a moderate influence on the G-matrix. Most part of the high energy tails of the thermal distributions are suppressed by the vertex form factors typically used to regularize the Bethe-Salpeter correlation integral. These expected properties are well reflected by our vertex functionals. The dependence of the vertices on chemical potential and temperature in Hartree approximation are illustrated in Fig. 5. The variations observed for high temperatures at chemical potentials close to the nucleon mass, are corresponding to the increased polarizability of low density nuclear matter. At these densities, the tails of the thermal distributions are not yet suppressed by the vertex form factors, hence leading to a stronger influence on the in-medium interactions. Note, that the iso-lines in Fig. 5 correspond to constant nuclear matter densities.

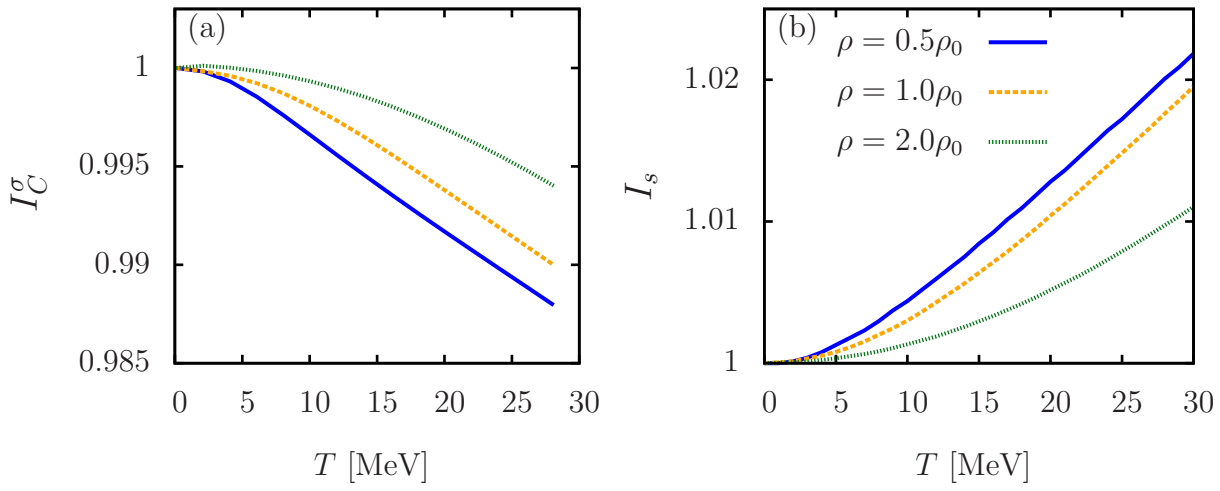


Figure 4: (Color online) Temperature dependence of the scalar coupling functions $I_C^\sigma$ (a) and $I_s^\sigma$ (b) at different densities: $\rho = 0.5\rho_0$ (blue line), $\rho = \rho_0$(orange dashed line), $\rho = 2\rho_0$ (green dotted), where $\rho_0$ is the saturation density at $T = 0$. Lower curves belong to lower densities.

In other studies the density-dependence of the meson-baryon vertices has been determined in a phenomenological approach, where the functional form of the vertices is adjusted to fit measured properties of symmetric and asymmetric nuclear matter and spherical nuclei. The first phenomenological description was introduced by Typel and Wolter [38]. The parameters were further adjusted to calculations of giant multipole resonances in [43] and [24]. Thus, in the present work we compare the results of the DDRH model to those obtained with the phenomenological DD-ME2 parametrization of the vertices as given in [24]. In order to better understand the effects arising from density depentent effective couplings, we also show some results for the linear Walecka model with constant couplings, which we refer to as QHD.

## IV. EQUATION OF STATE FOR ISOSPIN SYMMETRIC NUCLEAR MATTER

To begin with, we discuss our results for isospin symmetric nuclear matter at $T > 0$. An important quantity in the analysis of nuclear many-body properties is the binding energy per nucleon,

$$E_{\mathcal{B}} = \frac{\mathcal{E}}{\rho} - M, \tag{4.1}$$

with the total baryon density $\rho = \sum_b \rho_b$ and $M = \sum_b \frac{\rho_b}{\rho} M_b$. For the analysis of the different many-body effects it is helpful to separate $E_{\mathcal{B}}$ in a kinetic and a potential part, i.e. $E_{\mathcal{B}} = E_{\rm kin} + E_{\rm pot}$. By inserting $\mathcal{E}$ from Eq. 3.19 in the above equation and expressing the meson fields with the help of the corresponding self-energies, we can write

$$E_{\rm kin} = \frac{2}{\rho} \sum_b \left( \int \frac{\mathrm{d}^3 k}{(2\pi)^3} E^* \left( f_B + \bar{f}_B \right) - M_b^* \rho_b \right) \tag{4.2}$$

$$E_{\rm pot} = \frac{1}{2\rho} \sum_b \left( \Sigma_b^{0(0)} \rho_b - \Sigma_b^S \rho_b^s \right). \tag{4.3}$$

In Fig. 6 the results for the kinetic, potential and total binding energy per particle in the DDRH model are given as functions of the density for temperatures from 0 to 30 MeV. Obviously, thermal excitations affect mostly the kinetic part of the energy, while the potential energy is nearly unaffected by temperature effects. The kinetic energy is also modified by many-body interactions through the inclusion of the self-consistent effective masses $M_B^*$. At $T = 0$ this can be seen by comparing the DDRH result and the corresponding result for a non-interacting gas. The latter is indicated by the dashed curve in Fig. 6. Because the effective mass is decreasing with density, nucleon-nucleon interactions result in a repulsive effect in the kinetic energy.

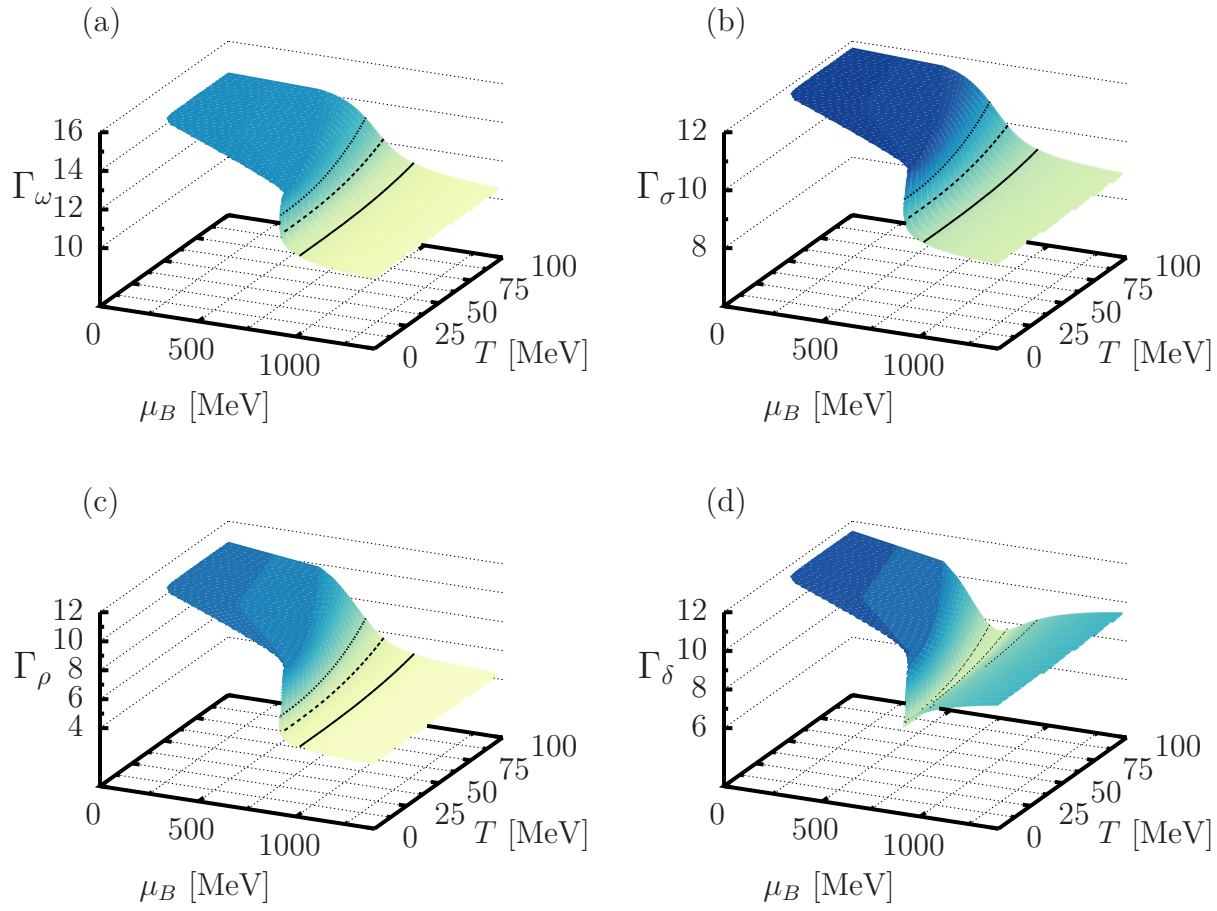


Figure 5: (Color online) Dependence of the Hartree mean-field vertices on chemical potential and temperature in symmetric nuclear matter. Results for the vector vertices $(\omega, \rho)$ and the scalar vertices $(\sigma, \delta)$, respectively, are displayed in the left and the right column, respectively. The dashed iso-lines indicate the constant density values of $0.5\rho_0$, $\rho_0$ and $2\rho_0$.

Table I: Comparison of the nuclear matter equilibrium properties at $T = 0$.

| Model | $\rho_0$ [fm$^{-}$3] | $E_{\mathcal{B}}(\rho_0)$ [MeV] | $K$ | $M_b^*$ | $E_{\rm sym}$ |
|---|---|---|---|---|---|
| DDRH | 0.181 | -15.94 | 282 | 518 | 26.7 |
| DD-ME2 | 0.153 | -16.54 | 251 | 534 | 32.3 |
| NL3 [25] | 0.148 | -16.3 | 272 | 562 | 37.4 |
| SLy230a [27] | 0.160 | -16.0 | 230 | 655 | 32.0 |
| QHD | 0.192 | -15.4 | 530 | 524 | 33.7 |

The repulsion of $E_{\rm kin}$ is partially compensated by the potential energy. $E_{\rm pot}$ is negative in the whole density range and decreases constantly with $\rho$. At lower temperatures the attraction of the potential energy is strong enough to create a binding in the total energy. The interplay between the repulsive and attractive character of the two energies shows up as a local minimum in $E_{\mathcal{B}}$, defining the saturation point $\rho_0$ of nuclear matter. In the DDRH calculation at $T = 0$ the saturation point is found at $\rho_0 = 0.18$ with $E_{\mathcal{B}}(\rho_0) = -15.94$, which is very close to DBHF calculations. A comparison of the equilibrium properties at $T = 0$ between the different models is given in Table I. With rising temperature the repulsion of $E_{\rm kin}$ becomes stronger leading to a less bound system. For $T > 22$ MeV $E_{\mathcal{B}}$ stays positive in the whole density range. In the $\rho \to 0$ limit the kinetic energy, and thus $E_{\mathcal{B}}$, comes very close to the classical value of an ideal gas, $E_{\mathcal{B}} = 3/2T$.

The effect of density-dependent interactions on the equation of state in the DDRH model can be better understood by examining the functional behavior of the rearrangement self-energy $\Sigma^R$. In Fig. 7 we show $\Sigma^R$ as a function of the

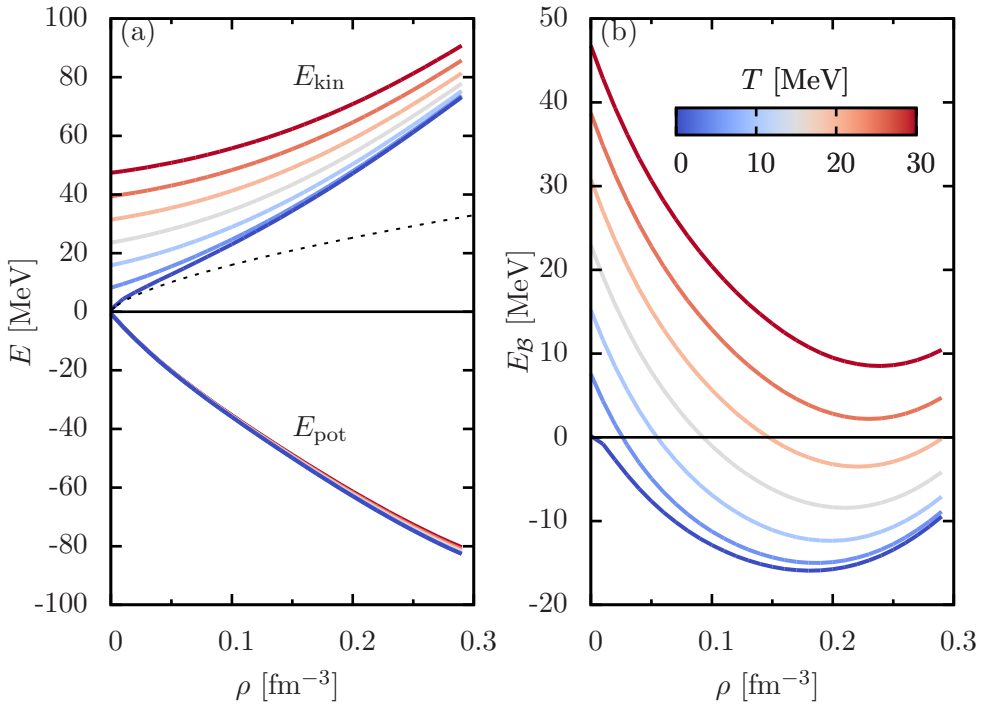


Figure 6: (Color online) (a) Density dependence of the kinetic (upper curves), potential (lower curves). (b) Binding energy per particle within the DDRH approach. Isotherms for temperatures T=0 to T=30 MeV in equidistant steps of 5 MeV are displayed. Note, that lower curves correspond to lower temperatures.

baryon density $\rho$ for symmetric nuclear matter at fixed temperatures. Obviously, $\Sigma^R$ is very small compared to the Hartree self-energies $\Sigma^{0(0)}$ ( $\approx$ 350 MeV at saturation density $\rho_0$). This justifies the expansion of the Hamiltonian up to the first order in the density deviation as described in the previous section. The temperature dependence of $\Sigma^R$ comes mainly from the scalar densities $\rho_b^s$ which saturate for $\rho \gg \rho_0$. Therefore, $\Sigma^R$ becomes independent of temperature in the high density limit. In the region of nuclear matter saturation density, $\rho_0$, the rearrangement contributions are more sensitive to temperature changes. However, the functional deviations are still rather small here and one can consider $\Sigma^R$ as independent of temperature for $T < 20$ MeV.

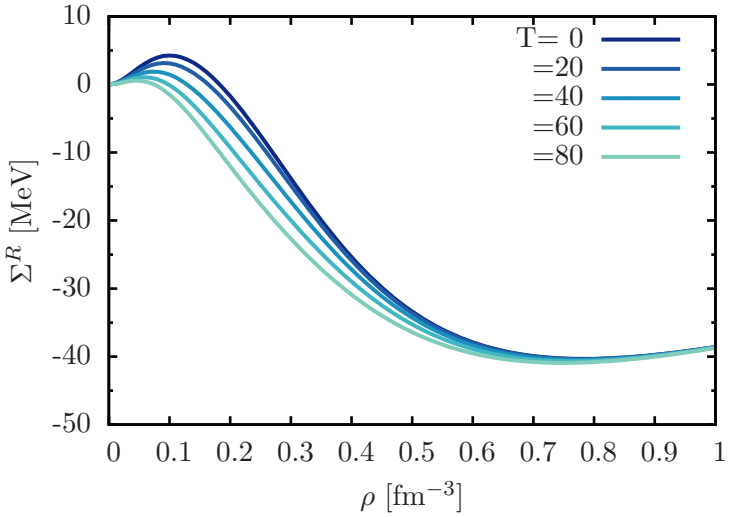


Figure 7: (Color online) The rearrangement self-energy $\Sigma^R$ as a function of baryon density $\rho$ at various values of temperature $T$ (in MeV). Lower curves correspond to higher temperatures.

The influence of the rearrangement energies on the pressure is illustrated in Fig. 8. The full DDRH calculation (solid lines) is compared to calculations without rearrangement terms (dashed lines). In contrast to the self-energies the rearrangement contributions have a significant effect on the nuclear matter pressure. Their modification on $P$ is even contrary in the low and high density region. While for $\rho < \rho_0$ the rearrangement terms cause an increase in the pressure density, their inclusion softens $P$ for $\rho > 1.5\rho_0$. This is of course a direct consequence of the functional dependence of $\Sigma^R$ on $\rho$ and $T$, since $P^R = \rho\Sigma^R$.

The increase of the pressure at low densities plays a crucial role on the liquid-gas phase transition region of nuclear matter. Figure 9 shows the pressure $P(T, \rho)$ of symmetric nuclear matter as a function of the nucleon density $\rho$ for

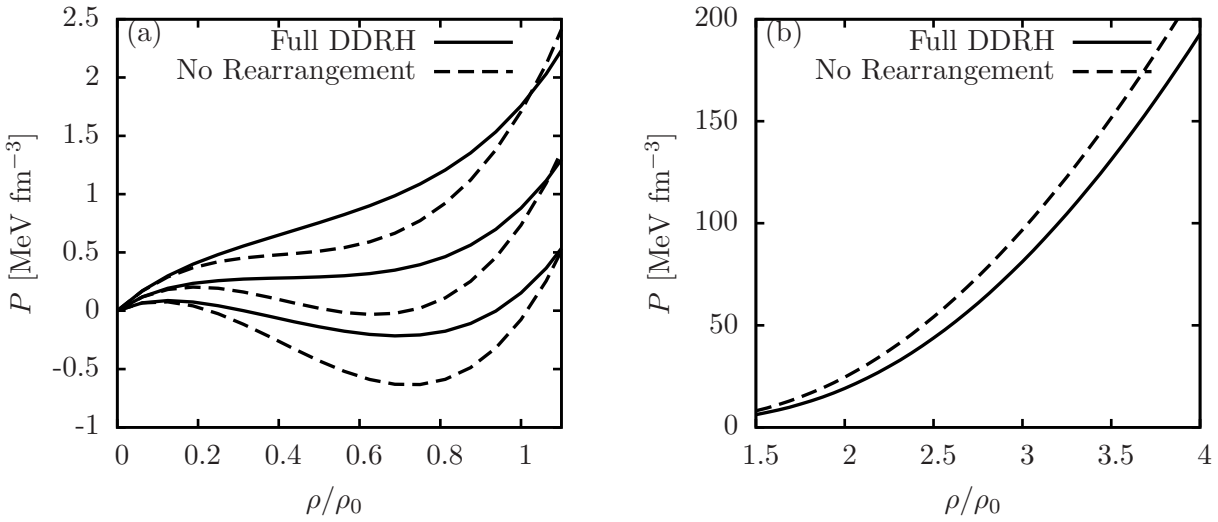


Figure 8: The rearrangement contributions to the pressure. (a) Low density region for $T = 10$, 15 and 20 MeV (lower curves correspond to lower $T$). (b) High density region for $T$ =20 MeV.

fixed values of the temperature $T$ (isotherms). The curves exhibit the characteristics of a typical first-order liquid-gas phase transition. In the low temperature region the pressure first increases slightly with the density, then decreases to its minimum point and finally returns to a continuous rising in the high density region, where it asymptotically approaches the causality limit $P = \mathcal{E}$ (Fig. 10). This functional behavior is very similar to the one of a classical van-der-Waals liquid [44].

Next, we discuss the entropy in the DDRH approach. Entropy production plays an important role in the determination of the mass fragment distribution in multi-fragmentation events of heavy-ion collisions [45]. In Fig. 11 the density and temperature dependence of the entropy per particle, $S/A = \mathcal{S}/\rho$, is shown. The left panel shows $S/A$ as a function of density for fixed temperatures in the range of 0-30 MeV. First of all we can see that the entropy increases with temperature and significantly decreases with density. This behavior is what is expected given the fact, that entropy is a measure of thermal disorder. At $\rho \to \infty$, $\mathcal{S}/\rho$ saturates at values in the range of 0.5-1.0 for the considered temperatures. Additionally, there are two notable limits. First, at low densities the entropy approaches the logarithmic density dependence of a classical system, $S/A \sim -\ln(\rho)$. This can be ascribed to the fact that in the regime of very low densities as well as high temperatures quantum effects become less important and thus the properties of a classical system are recovered. On the other hand, the temperature dependence of $S/A$ approaches a linear behavior at $T \to 0$, as shown on the right panel of Fig. 11. This becomes even more pronounced at higher densities. In this regime, the system can be assumed as a Fermi liquid, where the relation between $S$ is given by

$$\frac{\mathcal{S}_{\mathrm{FL}}}{A} = \frac{\pi^2}{2\rho} N_F T, \tag{4.4}$$

where

$$N_F = \frac{E_F k_F}{\pi^2} \tag{4.5}$$

is the density of states at the Fermi surface [46].

In Fig. 12 we compare the DDRH calculation of $S/A$ to results obtained from Au+Au collisions at energies between 100 and 400 AMeV [47]. The experimental data was obtained from the study of the fragments which remain after

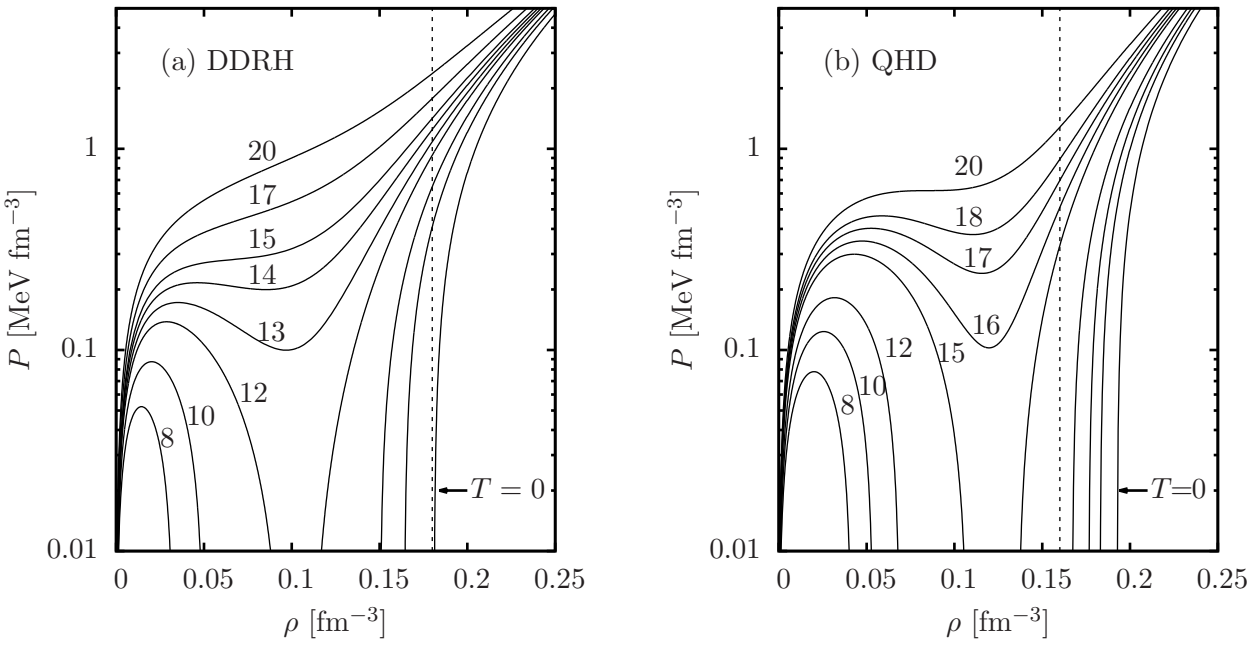


Figure 9: Comparison of the equation of state $P(\varepsilon(\rho)) = P(\rho)$ for symmetric nuclear matter at various temperatures. The numbers denote the temperature $T$ in MeV.

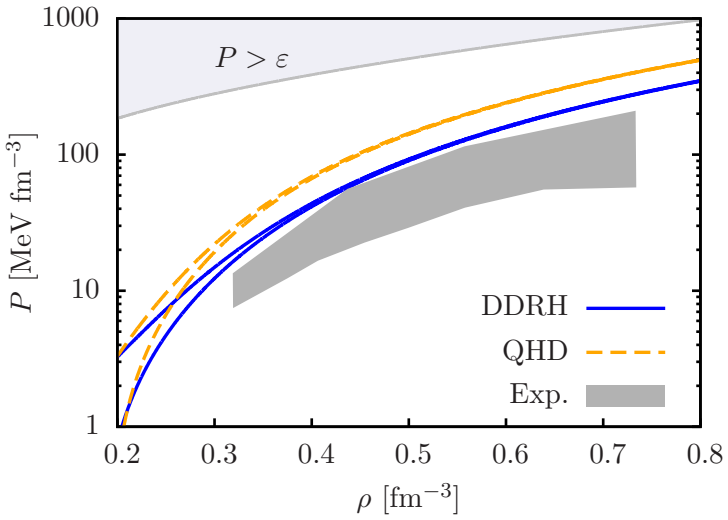


Figure 10: (Color online) Functional behavior of the pressure $P$ in the high density region for symmetric nuclear matter. The graph shows the results at $T = 0$ MeV (lower curves) and $T = 20$ MeV (upper curves) for DDRH and QHD models. The gray region corresponds to the region of pressures consistent with the experimental flow data. The upper blue shaded area, labelled by $P > \varepsilon$ exhibits the causality limit.

the collision. By assuming that the dense fireball created in the interior of a collision is in thermal equilibrium, information on the entropy per particle of the fireball can be obtained, in principle, from the fragmentation remnants of the collision, see e.g. [15]. However, this analysis comes with some uncertainties due to statistical assumptions which might not be fully satisfied in a heavy ion collision. Apart from that, one assumes that the freeze out density of the fireball is $\rho \approx .3\rho_0$. This provides a further uncertainty in the calculation. To account for small deviations from this central density we show the theoretical results in the range of $.047 \leq \rho \leq .053$ fm$^{-3}$. Although, we find that in this density and temperature range the differences between the DDRH and the simple QHD model are very small, the DDRH results indicate a slightly better agreement with the data for temperatures higher than

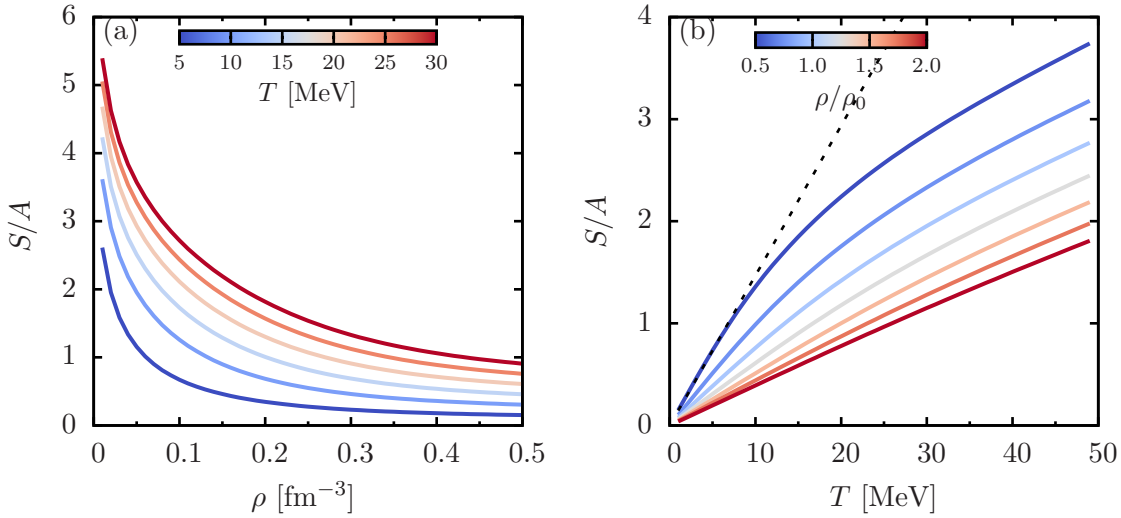


Figure 11: (Color online) Entropy per particle. Left: As a function of $\rho$ for fixed $T$ from 5 to 30 MeV in steps of 5 MeV. The dashed line shows the classical limit at T=30MeV. Right: As a function of $T$ for fixed density values from $0.5\rho_0$-$2\rho_0$ in steps of $\frac{1}{4}\rho_0$. The dashed line shows the limit of a Fermi liquid as explained in the text.

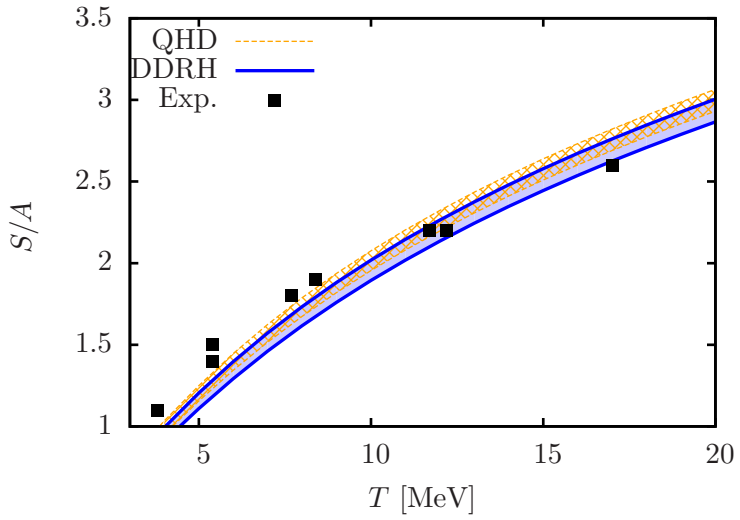


Figure 12: (Color online) Comparing the entropy per particle from the DDRH calculations to experimental results [47]. The theoretical band corresponds to $.047 \leq \rho \leq .053$ fm$^{-3}$, accounting for the uncertainties in the experimental analysis.

10 MeV. Nevertheless, one should note that a clear distinction between the models is barely possible for this set of data.

We conclude the set of results for symmetric nuclear matter with the discussion of the free energy per particle, $F/A = \mathcal{F}/\rho = (\mathcal{E} - T\mathcal{S})/\rho$. Fig. 13 shows $\mathcal{F}/\rho$ as a function of density and temperature. At very low temperatures the free energy has a local minimum, which is the equivalent to the saturation point of nuclear matter at $T = 0$. At finite temperatures the equilibrium state of the system is given by the minimization of the free energy instead of the energy density. This minimum describes a thermodynamically preferred state of the system. The local minimum of the free energy disappears above the so called flashing temperature, $T_{\rm F}$. At this point the pressure is still high enough to prevent the system from decaying to the low density (gas) phase, leading to a liquid-gas coexistence. Above a critical temperature, $T_C$, this coexistence does not hold any longer and the system is found in the thermodynamically preferred state at very low densities. For the DDRH model we find the following values for the flashing and critical temperatures of symmetric nuclear matter:

$$T_F^{\rm DDRH} \approx 12.2, \quad T_C^{\rm DDRH} \approx 14.6.$$

Although $E/A$ is more repulsive with rising temperature, the free energy per particle is a decreasing function of $T$. Obviously, this behavior can be ascribed to the $-T\mathcal{S}$ term and thus is a pure entropic effect. The same applies to the $\rho \to 0$ limit, where classical effects dominate the properties of the system (compare Fig. 11) [48].

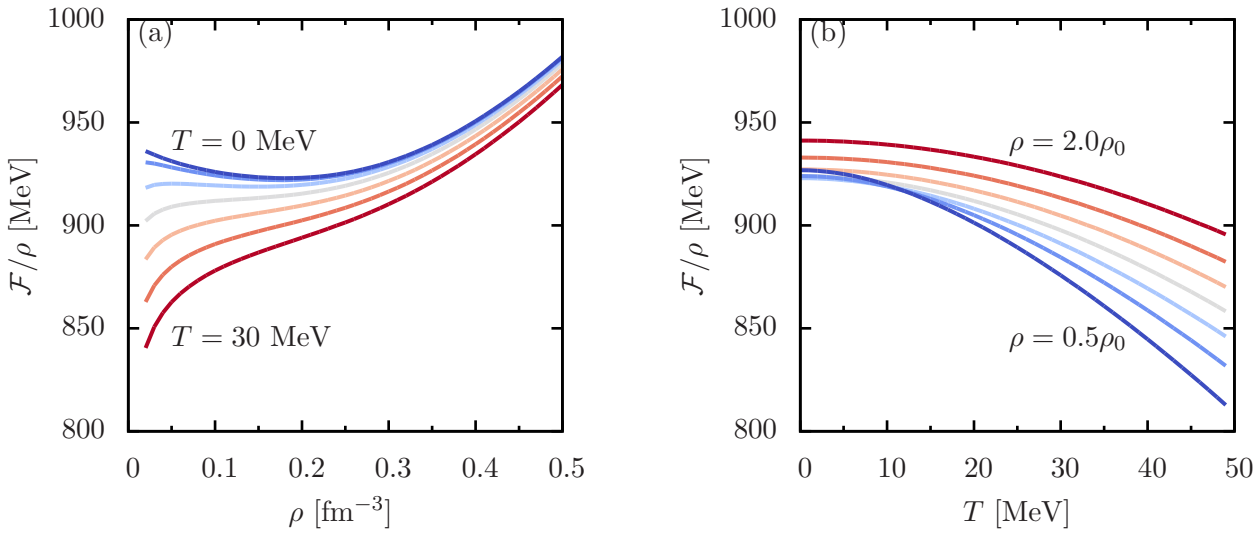


Figure 13: (Color online) The free energy per particle. Isotherms are chosen the same as Fig. 11.

The analysis of symmetric nuclear matter shows that nucleon-nucleon interactions affect the bulk properties of nuclear matter in two ways. First, they obviously give rise to the potential energy. Second, the interactions invoke self-consistent effective masses and chemical potentials. Especially the latter quantities affect both the thermal and spectral distributions functions of the nucleons. Therefore, the in-medium interactions have a remarkable effect on the kinetic part of the (free) energy, effectively increasing the kinetic energy.

In the considered density and temperature range, our results for the DDRH model are in good agreement with experimental data as well as other microscopic DBHF calculations [41]. This shows, that the approximations applied here to the density-dependent vertices are not only suitable for the description of nuclear matter in the vicinity of the saturation point at $T = 0$, but lead also to reliable results in higher density as well as temperature regions.

## V. ISOSPIN ASYMMETRIC NUCLEAR MATTER

### A. Thermal Properties of Asymmetric Nuclear Matter

In the previous section we studied the results for nuclear matter with equal content of protons and neutrons. In this section we study isospin effects in warm nuclear matter at moderate temperature well below the critical temperature $T_C$ of the QCD phase transition. For this purpose, we introduce the proton fraction $\xi \equiv \rho_p/\rho$ as an indicator for charge asymmetry and the isospin content. In the DDRH model, the inclusion of the scalar isovector $\delta$ meson field leads to a separation of the proton and neutron effective masses in asymmetric nuclear matter. In Fig. 14 we plot the ratio between the effective and the corresponding bare nucleon mass. The black dashed curve on the left panel shows the result for symmetric nuclear matter ($\xi = 0.5$). In this case $M_p^* = M_n^*$ decreases continuously with $\rho$. As the asymmetry increases (i.e. smaller values of $\xi$), protons gain a larger effective mass, while the effective mass of neutrons decreases. It is particularly interesting to note, that the isospin effect on $M_p^*$ is much stronger than on $M_n^*$. In the limit of $\xi = 0$ (neutron matter) $M_n^*$ deviates only slightly from its symmetric nuclear matter value, whereas $M_p^*$ shows a considerable increase and even exhibits a local minimum at $\rho \approx 2.3\rho_0$. This behavior is a direct consequence of the self-consistent solution of the effective masses and scalar densities.

Fig. 15 shows the energy density and pressure at $T = 0$ for values of $\xi$ from pure neutron matter ($\xi = 0$) to symmetric matter ($\xi = 0.5$. As seen, the local minimum of the binding energy per particle shifts to the left, i.e. to

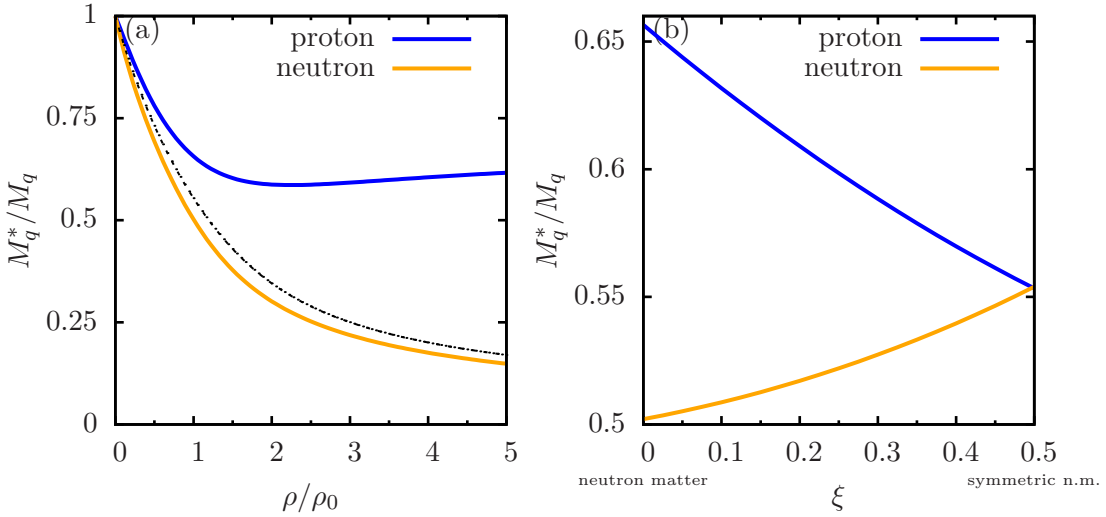


Figure 14: (Color online) Effective nucleon masses $M_q^*$ $(q = p, n)$ for protons (upper blue) and neutrons (lower orange) at $T = 0$ as functions of the total baryon density for pure neutron matter (left) and as functions of the asymmetry parameter $\xi = \frac{Z}{A}$ at saturation density $\rho = \rho_0$ (right). The thin dashed curve in the left panel represents the result in case of symmetric nuclear matter.

lower densities, while the binding of the system reduces with increasing neutron excess. For $\xi < .05$ neutron-rich matter is completely unbound. At this point the potential energy is not strong enough to compensate the kinetic energy of the system. Hence, both, energy density and pressure increase with decreasing proton fraction. In neutron-rich matter, the local minimum of the pressure disappears as well, as the right panel of Fig. 15 shows. Thus, the thermodynamically preferred state of neutron matter is a dilute Fermi gas in the entire density range.

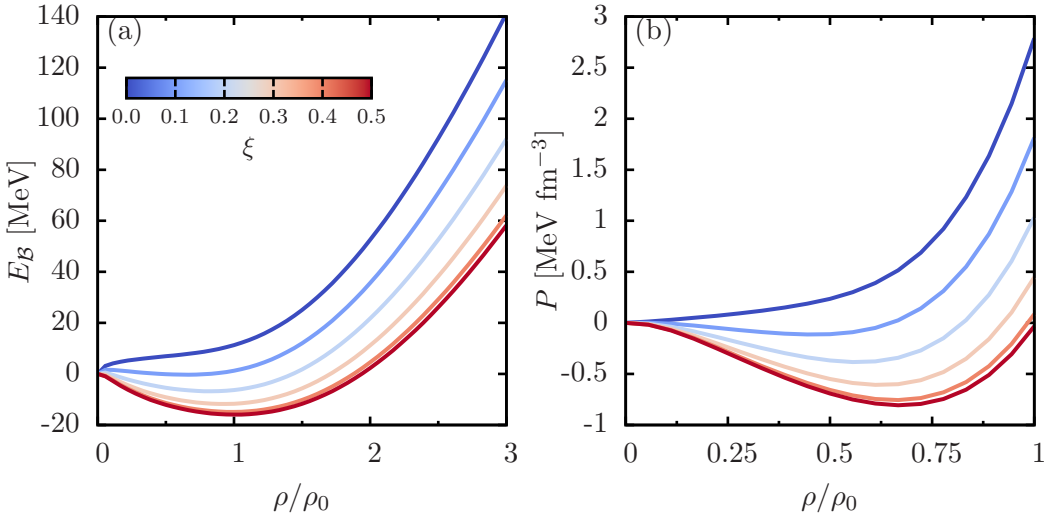


Figure 15: (Color online) The binding energy (left) and the pressure (right) at $T = 0$ for values of $\xi$ from 0 to .5 in steps of 0.1. Lower curves belong to lower values of $\xi$.

The entropy $S/A$ decreases for smaller values of $\xi$ as the degrees of freedom are reduced in systems with smaller proton fractions. In our calculations, we find a very similar asymmetry dependence of $S/A$ in the whole temperature range. As an example, we show $S/A$ as a function of $\xi$ within several models at a fixed temperature of $T = 10$ MeV. The results show that the calculation with the linear QHD parametrization produces somewhat larger values of the entropy. The blue solid curve of the DDRH calculation lies above the results with the phenomenological DD-ME2 parametrization [24]. This difference is less pronounced at smaller $\xi$, however, and at neutron matter the entropy in the DDRH model is even slightly smaller than the one of the DD-ME2 calculation. In the right panel of Fig. 16 we

compare the entropy per particle as a function of the temperature between symmetric nuclear matter and neutron matter within the DDRH model. For neutron matter $S/A$ shows a linear temperature dependence throughout almost the whole temperature range.

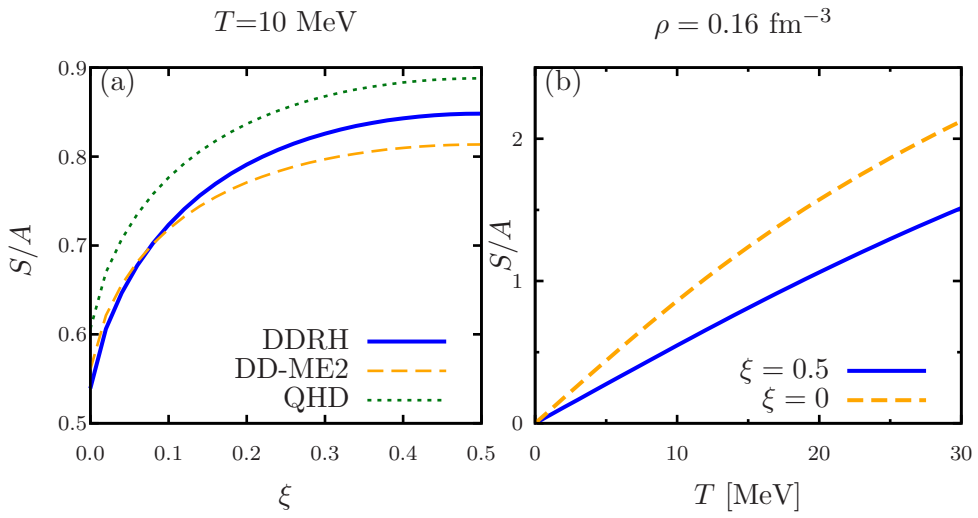


Figure 16: (Color online) Left: The entropy per particle as a function of the proton fraction $\xi$ at $T$=10 and $\rho$=0.16 fm$^{-3}$. The results for the DDRH, DD-ME2 [24] and QHD parametrization are shown. Right: Comparison of the temperature dependence of the entropy per particle between symmetric (upper curve) and pure neutron matter (lower curve) in the DDRH model at fixed density $\rho = 0.16$ fm$^{-3}$.

In Fig. 17 the free energy per particle of neutron matter is compared between the DDRH and the phenomenological DD-ME2 model. The results show that the DDRH parametrization leads to a less repulsive free energy which is a consequence of the additional attraction in the scalar-isovector channel. At low densities the curves of the two models coincide with each other, since the differences between the interactions become less important in this density region. As in the case of symmetric nuclear matter, $F/A$ decreases with temperature due to the higher values of the entropy.

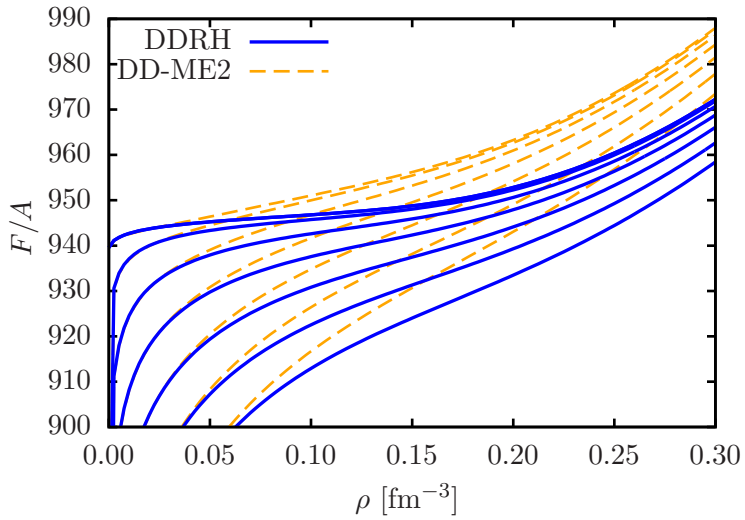


Figure 17: (Color online) Free energy per particle in neutron matter for temperatures from 0 to 30 MeV in equidistant steps of 5 MeV (lower curves correspond to higher temperatures). The results of the DDRH (solid lines) and the DD-ME2 (dashed lines) model are compared.

To investigate the isospin dependent part of the equation of state, consider the expansion of the free energy in

Table II: $E_{\rm sym}$ and $F_{\rm sym}$ taken at saturation density for different values of temperature $T$ in the DDRH and DD-ME2 model.

| T [MeV] | $E_{\rm sym}^{\rm DDRH}$ [MeV] | $E_{\rm sym}^{\rm DD-ME2}$ [MeV] | $F_{\rm sym}^{\rm DDRH}$ [MeV] | $F_{\rm sym}^{\rm DD-ME2}$[MeV] |
|---|---|---|---|---|
| 10 | 26 | 32 | 27 | 33 |
| 20 | 24 | 30 | 29 | 35 |
| 30 | 21 | 28 | 32 | 37 |
| 40 | 19 | 26 | 36 | 41 |
| 50 | 17 | 25 | 41 | 45 |

powers of the isospin parameter $\alpha \equiv (\rho_n - \rho_p)/\rho$ around symmetric nuclear matter ($\alpha$=0):

$$F(\alpha, \rho, T) = F(0, \rho, T) + F_{\rm sym}(0, \rho, T)\alpha^2 + \mathcal{O}(\alpha^4). \tag{5.1}$$

Because of isospin symmetry, odd powers of $\alpha$ vanish in the above expansion. Eq. 5.1 defines the free symmetry energy, $F_{\rm sym}$, which is related to the cost of converting protons into neutrons in the nuclear medium. Accordingly, the symmetry energy, $E_{\rm sym}$, and the symmetry entropy, $S_{\rm sym}$, can be defined in the same way. The relation to the proton fraction parameter $\xi$ is then given by

$$A_{\rm sym} = \frac{1}{8}\frac{1}{\rho}\frac{\partial^2 \mathcal{A}}{\partial \xi^2}\bigg|_{\xi=0.5}, \quad \mathcal{A} \in \{\mathcal{F},\ \mathcal{E}, \mathcal{S}\} \tag{5.2}$$

As usual, the above symmetry functionals follow the general thermodynamic relation $F_{\rm sym} = E_{\rm sym} - TS_{\rm sym}$.

The symmetry energy plays a fundamental role in the description of many important phenomena in nuclear physics, such as the structure of exotic nuclei, heavy ion collisions and neutron stars. In the past decade the density dependence of the symmetry energy has been extensively studied both experimentally and theoretically [49]. In addition, the knowledge of the temperature dependence of the (free) symmetry energy has become more and more important in connection with the analysis of multi-fragmentation data of hot nuclear matter. It is also an important ingredient in astrophysical calculations such as the evolution of proto-neutron stars or the core collapse of a massive star and the associated explosive nucleo-synthesis [50, 51]. In the last years some progress has been achieved in heavy ion collision experiments to extract the temperature dependence of $F_{\rm sym}$ at low densities [52].

In Fig. 18 we show our prediction for $F_{\rm sym}$ and $E_{\rm sym}$ (see also Table II). Again, results for DDRH and DD-ME2 parameter sets are compared together with the experimental data points from charge exchange reactions [53], neutron skin analysis [54] and heavy ion collisions [55]. The symmetry energy of the DDRH model shows a stiff density dependence, while it is soft for the phenomenological DD-ME2 model parameter set. At $T$=0 and at low densities both models describe the experimental data quite well. At saturation density the DDRH parametrization slightly underestimates the experimental value for $E_{\rm sym}$. However, since – different to the DD-ME2 model – the DDRH parameter set has not been fitted to experimental data this result is already quite noteworthy. As for the temperature dependence, one can see that $F_{\rm sym}$ and $E_{\rm sym}$ show an opposite behavior. While $F_{\rm sym}$ increases with $T$, $E_{\rm sym}$ becomes smaller with rising temperature. The decrease of $E_{\rm sym}$ at higher temperatures can be understood from the fact that the Fermi surface is more diffuse and therefore the Pauli blocking becomes less important at increasingly higher temperatures. The increase of the free symmetry energy, however, is related to the negative value of $S_{\rm sym}$, since the total entropy per particle decreases with increasing asymmetry (Fig. 16). Consequently, $F_{\rm sym}$ is expected to be larger than $E_{\rm sym}$ at fixed density and temperature values. Additionally, the entropic effect of the free symmetry energy is stronger than the decrease of $E_{\rm sym}$ which all in all causes $F_{\rm sym}$ to increase with $T$.

### B. Phase Transitions in Asymmetric Nuclear Matter

As a starting point, let us first recall some basic concepts of phase transitions in nuclear matter. The equation of state of nuclear matter shows a typical van-der-Waals gas behavior at temperatures $0 < T < 20$ MeV [44]. Below a critical temperature $T_C$ one finds a region where $\frac{\partial P}{\partial \rho}\Big|_T < 0$. This is the region of mechanical instability where the preferred state of the system is given by two coexisting phases. The thermodynamical equilibrium of the two phases can be obtained with the help of the Gibbs-Duhem relation,

$$\mathrm{d}P - \mathcal{S}\mathrm{d}T - \sum_c \rho_c \mathrm{d}\mu_c = 0, \tag{5.3}$$

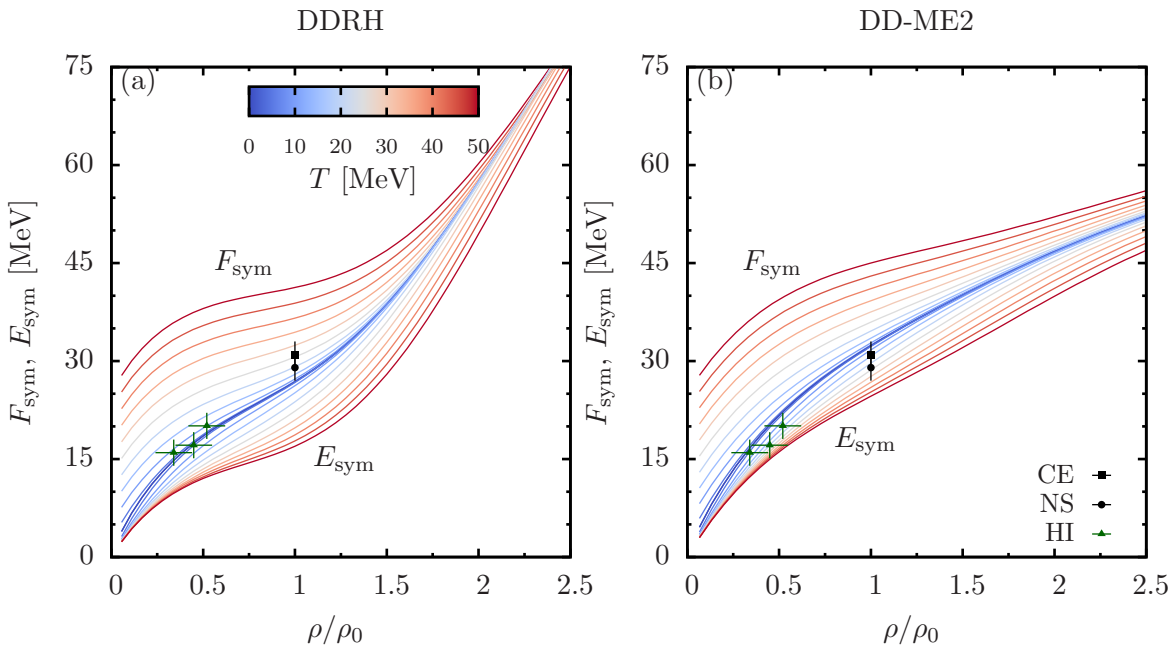


Figure 18: (Color online) Symmetry and free symmetry energy as functions of the density for fixed values of $T$ from 0 to 50 MeV. At $T$=0 (blue curve) $F_{\rm sym} = E_{\rm sym}$. Curves above (below) the zero temperature line correspond to $F_{\rm sym}$ ($E_{\rm sym}$). The right and the left panel show the results for the DDRH and DD-ME2 model, respectively. The points indicate experimental results for the symmetry energy at $T$=0. The data points are taken from [53] (CE) , [54] (NS) and [55] (HI)

where the sum includes all conserved charges. Eq. (5.3) applies to both phases separately. In case of one conserved charge this leads to the Gibbs conditions

$$\mu^I(\rho^I, T) = \mu^{II}(\rho^{II}, T), \tag{5.4}$$
$$P^I(\rho^I, T) = P^{II}(\rho^{II}, T), \tag{5.5}$$

where the labels $I$ and $II$ refer to the two phase-states, with the convention $\rho^I < \rho^{II}$. Recalling that the preferred state of a system is the one with the lowest value of the free energy, we can write down the global stability condition for the mixed phase [9]:

$$\mathcal{F}(\rho, T) < \lambda\mathcal{F}(\rho^I, T) + (1-\lambda)\mathcal{F}(\rho^{II}, T), \tag{5.6}$$

with

$$\rho = \lambda\rho^I + (1-\lambda)\rho^{II} \quad \lambda \in [0, 1],$$

where the parameter $\lambda$ determines the volume fraction occupied by each phase. Eq. (5.6) implies that for a stable system $\mathcal{F}$ should be a convex function of the density,

$$\frac{\partial^2 \mathcal{F}}{\partial \rho^2} \geq 0.$$

Note, that the above expression is equivalent to $\frac{\partial \mu}{\partial \rho} \geq 0$, as can be easily deduced from $\mathrm{d}\mathcal{F} = -\mathcal{S}\mathrm{d}T + \sum_c \mu_c \mathrm{d}\rho_c$. With this, the phase transition region is characterized by the following states,

- *spinodal curve*: describes the onset of the instability region, $\frac{\partial^2 \mathcal{F}}{\partial \rho^2} = 0$
- *metastable region*: the stability conditions are fulfilled locally, but Eq. (5.6) is violated
- *binodal curve*: describes the onset of the metastable states.

Hence, the two-phase coexistence area is enclosed by the binodal curve. Within this area the pressure and the chemical potentials are kept constant. The projection of the coexistence area onto the $T$-$P$ or $T$-$\mu$ plane results in the first-order phase transition lines. Together with the $T$-$\rho$ phase diagram they provide a full description of the phase transition. In Fig. 19 we present the DDRH results of the $T$-$\rho$ (left) and the $T$-$P$ (right) phase diagrams. The hatched area indicates the region of mechanical instability. We find a critical temperature of $T_C \approx 14.55$ MeV. The calculation with the DD-ME2 parameter set provides similar results, although the values of the critical points are a bit smaller than in the DDRH case.

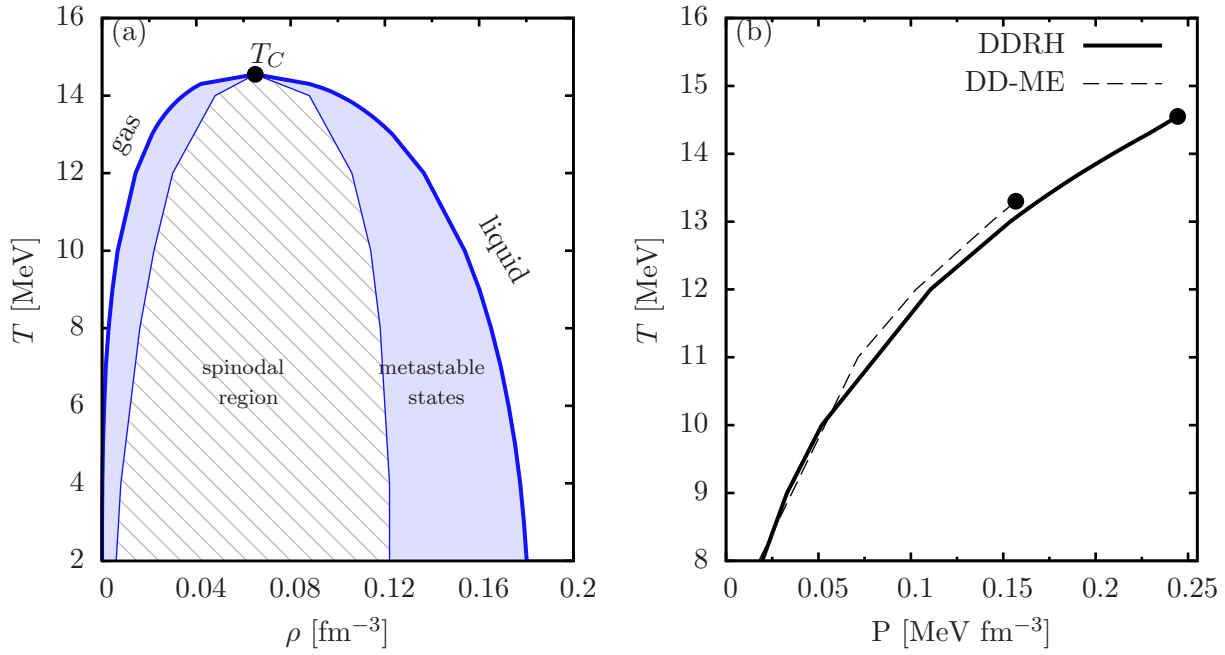


Figure 19: (Color online) The phase transition diagrams of symmetric nuclear matter. Left: The $T$-$\rho$ phase diagram in the DDRH model. The binodal and spinodal curves are indicated by thick and thin lines, respectively. Right: The $T$-$P$ phase diagram for the DDRH and DD-ME2 model calculations.

The above conditions can be generalized to describe phase transitions of multi-component systems with $N$ conserved charges, e.g. hyper nuclear matter. The stability criterion (5.6) then holds for each conserved charge density $\rho_i$. The resulting set of $N$ inequalities implies [9]

$$\frac{\partial \mu_i}{\partial \rho_j} = \frac{\partial \mu_j}{\partial \rho_i} > 0 \tag{5.7}$$

In the coexistence region the Gibbs conditions of a multi-component system have to be fulfilled for each particle type,

$$\mu_i(\rho_i^I) = \mu_i(\rho_i^{II}), \quad P(\rho_i^I) = P(\rho_i^{II}). \tag{5.8}$$

For isospin asymmetric nuclear matter the conserved charges of the system are given by the baryon number $B$ and the third component of the total isospin $I_3$. Any state of the nuclear matter system can thus be characterized by the baryon density $\rho_B{=}\rho_p + \rho_n$ and the isovector density $\rho_3 = \rho_p - \rho_n$. The corresponding baryon and isospin chemical potentials are related to the nucleon and proton chemical potentials through

$$\mu_B = \mu_p + \mu_n, \quad \mu_3 = \mu_p - \mu_n.$$

It is feasible to express the stability conditions in terms of the proton fraction $\xi$,

$$\rho \left(\frac{\partial P}{\partial \rho}\right)_{T,\xi} > 0, \quad \left(\frac{\partial \mu_p}{\partial \xi}\right)_{T,P} > 0, \quad \left(\frac{\partial \mu_n}{\partial \xi}\right)_{T,P} < 0. \tag{5.9}$$

The last two expressions are referred to as *chemical stability* conditions. They take into account the fact that there is energy needed to change the concentration of protons in the medium at a fixed temperature and pressure. The

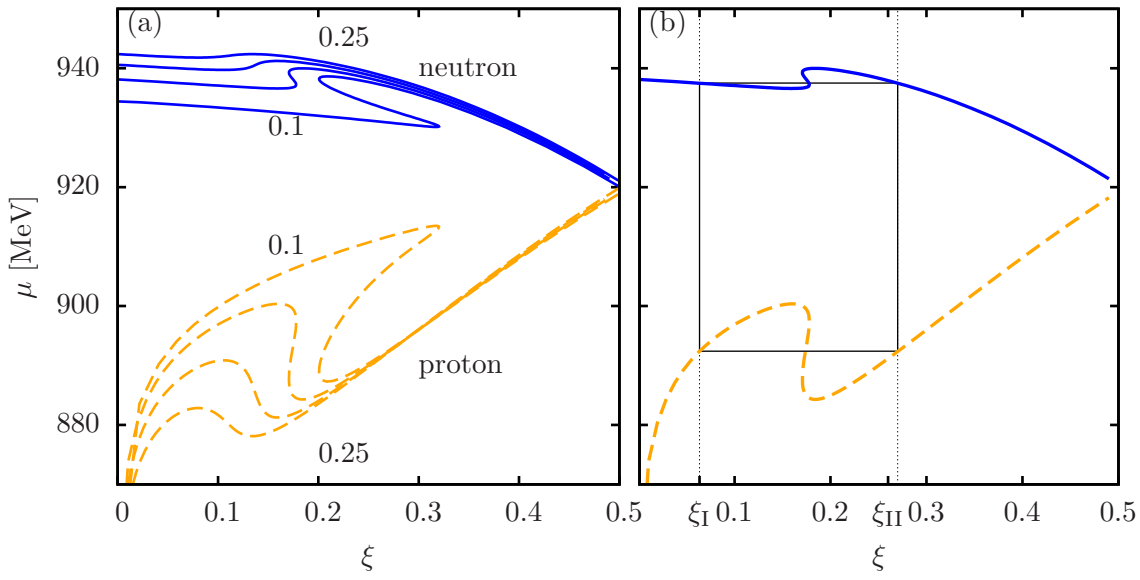


Figure 20: (Color online) The chemical potential isobars of nuclear matter in the DDRH model as a function of $\xi$ at $T = 10$ MeV. The left panel shows the neutron (solid blue) and proton (dashed orange) isobars for values of $P$ from 0.1 to 0.25 MeV fm$^{-3}$. The right panel indicates the geometrical construction in case of $P$=0.15 MeV fm$^{-3}$ as described in the text.

chemical instability region is found from the analysis of the neutron and proton chemical potential isobars as functions of $\xi$. In Fig. 20 a set of isobars in the range of 0.1 MeV fm$^{-3}$ $< P <$ 0.25 MeV fm$^{-3}$ is shown. One can see an area in the $P$-$\xi$ space, where the chemical stability conditions are violated. In this section the system would break apart into two phases with different concentrations of its constituents. With increasing pressure the instability region becomes smaller until it disappears completely at the critical pressure $P_C$. At this point an inflection point appears in the chemical potential isobars,

$$\left(\frac{\partial\mu}{\partial\xi}\right)_{T,P=P_C} = \left(\frac{\partial^2\mu}{\partial\xi^2}\right)_{T,P=P_C} = 0$$

In models with constant nucleon-meson couplings the position of the inflection points of protons and neutrons coincides in the $P$-$\xi$ plane. This assumption is, however, no longer true, once the couplings become density dependent. In this case, the chemical potential of one type of nucleons can pass an inflection point while the other one still has an unstable region. This circumstance was first found by Qian [56] where it was shown that the asynchronous behavior of the nucleon specie varies according to the density dependence of the isovector-vector coupling, $\Gamma_\rho$. In agreement with that, we find a similar situation for the DDRH model.

In phase equilibrium, the pressure and the chemical potentials of the two phases are equal, as required by the Gibbs conditions. The two solutions to this requirement can be found by means of a geometrical construction, as shown in the right panel of Fig. 20 [57]. The points $\xi_{\rm I}$ and $\xi_{\rm II}$ indicate the onset of the coexistence region. Thus, owing to the additional degree of freedom, the binodal curve becomes a surface in the $T$-$P$-$\xi$ space. To better visualize this surface, it is usually displayed in slices at constant $T$, which is referred to as the *binodal section*. The shape of the binodal section depends highly on the model of the nucleon-nucleon interaction.

To illustrate the nature of the liquid-gas transition in asymmetric nuclear matter, we show the result of the binodal section of the DDRH model at $T$=10 MeV in Fig. 21. Following the notation of [9], we indicate some characteristic points of the curve. By *MA* the point at maximum asymmetry is indicated. For $\xi < \xi_{\rm MA}$ the system stays in the gas phase and a phase transition does not take place. The point of equal concentration, *EC*, lies at $\xi = 0.5$, reflecting the one-component character of symmetric nuclear matter. The critical point $CP(\xi_C, P_C)$ indicates the edge of the instability area. For $P > P_C$ the chemical potentials of protons and neutrons are monotonically with $\xi$.

In the phase coexistence region the system favors a configuration with different proton concentrations of the two phases. This does not violate the isospin conservation law, since only the sum of the isospin of the two phases needs to be conserved. One finds, that the phase with lower $\xi$ (higher asymmetry) takes the lower density. The points *CP* and *EC* divide the binodal section into two branches, where the left(right) branch corresponds to the phase with lower(higher) density and proton concentration. Thus, the left branch is associated with the gas phase and the right

one with the liquid phase. The binodal section shrinks with temperature, i.e., $P_{\rm CP}$ becomes smaller and $MA$ shifts to higher values of $\xi$. At $T$=$T_C$ the points $CP$, $MA$ and $EC$ coincide at $\xi = \frac{1}{2}$ and the binodal surface finally reduces to a single point.

In contrast to symmetric nuclear matter, the pressure does not stay constant during a phase transition. This arises from the fact that the two phases follow the two different branches along the binodal curve. As an example, consider a system in a configuration below the binodal section with $\xi$=0.2. As the system is isothermally compressed, it will reach the two-phase instability region at the point $A_1$. In this stage a second phase emerges at the point $B_2$ with $\xi \approx$0.4 (liquid phase). During the phase transition the total proton fraction $\xi$ is held fixed, as indicated by the vertical line in the left panel of Fig. 21. The two coexisting phases evolve along the two different branches of the binodal section. The gas phase follows the left branch from $A_1$ to $A_2$ and the liquid phase follows the right branch from $B_1$ to $B_2$. Finally, the system leaves the instability area at the point $B_2$. The solution of the equations

$$\rho = \lambda\rho^{\rm I} + (1-\lambda)\rho^{\rm II}$$

$$\rho_3 = (2\xi - 1)\rho = \lambda\rho_3^{\rm I} + (1-\lambda)\rho_3^{\rm II}$$

provides the fraction $\lambda$ of the volume which is occupied by the gas phase. In the above example, $\lambda$=1 at $A_1$ and vanishes at $A_2$, implying that the system evolves from a gas to a liquid phase. The solution of the above equations can be used to calculate the behavior of the pressure during the phase transition. This is illustrated in the right panel of Fig. 21.

The behavior of the system during an isothermal compression can be very different depending on the asymmetry parameter. In general, one can distinguish between the following two condensation types

- $\xi > \xi_s$: stable condensation
  starting in the gas phase, the system undergoes a phase transition and ends in the stable liquid phase.
- $\xi < \xi_s$: retrograde condensation
  The system starts and terminates its evolution through the two-phase coexistence region in the gas phase. The liquid phase which emerges during the transition disappears again as the upper boundary of the binodal section is reached. This behavior does not occur in a one-component system.

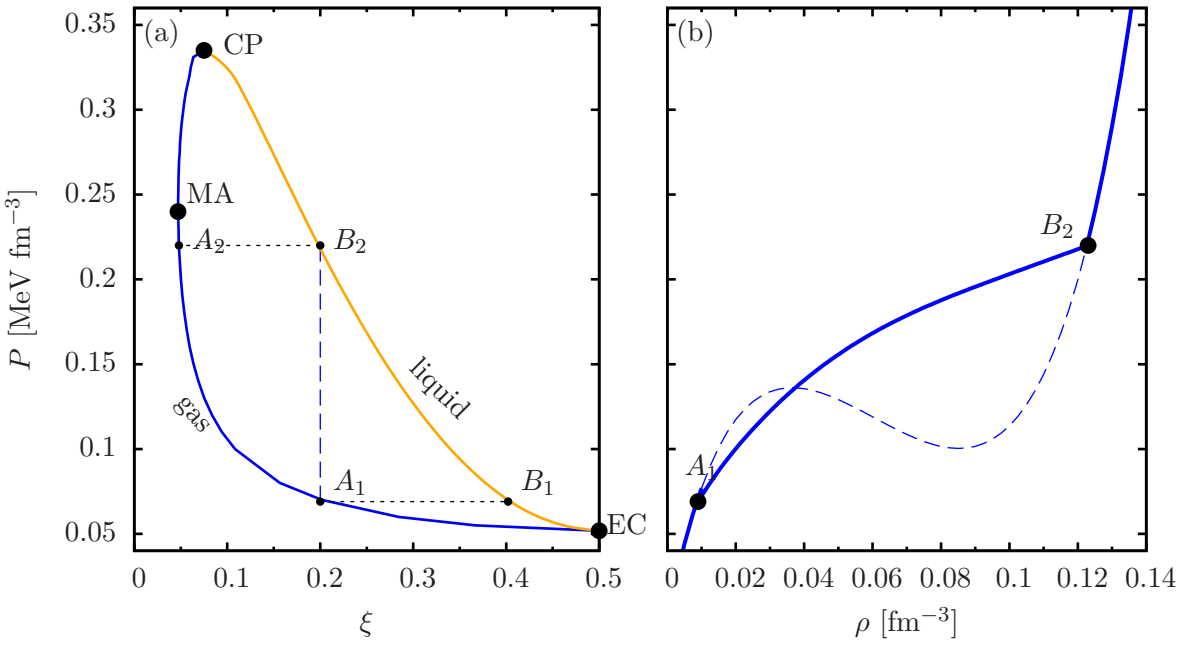


Figure 21: (Color online) The binodal section at $T$=10 MeV in the DDRH model. The right panel shows the projection of the points $A_1$ and $A_2$ on the pressure at fixed proton concentration $\xi = 0.2$.

It is interesting to examine, how the shape of the binodal section depends on the nucleon-nucleon interaction. Especially the position of the characteristic points is very sensitive to the isospin part of the interaction. In Fig.

Table III: Comparison of the critical point parameters for several temperatures. The results for the NL3 and SLy230a models are taken from [10]

| | T [MeV] | $\xi_c$ | $\rho_c$ [fm$^{-3}$] |
|---|---|---|---|
| DDRH | 0 | 0.0135 | 0.059 |
| DD-ME2 | 0 | 0.0025 | 0.0327 |
| NL3 | 0 | 0.0567 | 0.0766 |
| SLy230a | 0 | 0.0149 | 0.0843 |
| DDRH | 10 | 0.077 | 0.079 |
| DD-ME2 | 10 | 0.167 | 0.065 |
| NL3 | 10 | 0.1785 | 0.0573 |
| SLy230a | 10 | 0.110 | 0.0608 |
| DDRH | 14.55 | 0.5 | 0.0653 |
| DD-ME2 | 13.31 | 0.5 | 0.045 |
| NL3 | 14.55 | 0.5 | 0.0463 |
| SLy230a | 16.52 | 0.5 | 0.0535 |

22(a) the binodal section at $T$=10 MeV of the DDRH model is compared to the results from other models. A summary of the corresponding critical values can be found in Tab. III.

As in the case of symmetric nuclear matter, density dependent interactions provide a much smaller coexistence region. In the QHD model the instability region extends to $P \approx 0.56$ MeV fm$^{-3}$. The DDRH binodal stretches to much smaller values of the asymmetry parameter $\xi$ than the one of the phenomelogical DD-ME2 model. The point of maximum asymmetry is found at $\xi_{\rm MA} \approx 0.05$ and $\xi_{\rm MA} \approx 0.1$ in the DDRH and DD-ME2 case, respectively. We also display the result of the non-relativistic Skyrme type interaction SLy230a by Dutra et al. [10]. The DD-ME2 binodal is remarkably close to the one of the SLy230a model. This circumstance can be related to the way the isovector channel is parametrized in the corresponding models, as was also found by Dutra et al. To illustrate this more clearly, we show in Fig. 22(b) the impacts of the isovector-scalar $\delta$ channel and the momentum correction in the DDRH model on the binodal shape. The dashed curve represents the result without the $\delta$ meson interaction, where $\Gamma_\delta$=0. One can see that the $\delta$ interaction increases the value of the maximum asymmetry. The short dashed line represents the solution without momentum corrections, where we set all momentum correction parameters ($C_S$) to zero. One can see, that momentum correction leads to lower values of $\xi_{\rm MA}$ by approximately the same extent as of the $\delta$ interaction. It is also interesting to note, that the binodal section of the DD-ME2 and SLy230a model is very close to the one of the DDRH model without momentum correction terms.

In conclusion to this discussion, we study the asymmetry dependence of the critical temperature. First of all we should remark that in case of asymmetric nuclear matter the definition of the critical temperature is used differently in literature [58]. Some authors define the critical temperature for a given value of $\xi$ such, that $\xi$ corresponds to $\xi_C$ at $T$=$T_C$. In this way the system remains in the gas phase for $T > T_C$ [59]. On the other hand, many authors prefer the definition which is equivalent to the one of symmetric nuclear matter, that is, where the pressure has an inflection point in the $P$-$\rho$ phase diagram. This definition represents the temperature, from which the system remains mechanically stable, albeit a chemical instability may still be present at this point. Therefore, one should rather refer to this temperature as the critical temperature of mechanical instability, $T_{\rm CM}$. Since the calculation of $T_{\rm CM}$ is more straightforward and also more familiar, it is widely used in the literature [48, 60, 61]. $T_{\rm CM}$ is somewhat smaller than $T_C$, yet it also represents the asymmetry dependence of the instability region.

In Fig. 23 we show the mechanical critical temperature as a function of $\xi$ for different models. $T_{\rm CM}$ decreases continuously with rising neutron excess and vanishes at $\xi$=$\xi_{\rm CM}$. For asymmetry fractions below this value, the system remains mechanically stable at all temperatures. At higher values of $\xi$ the curve of the QHD model lies above the curves of the other models, overshooting the experimental value of symmetric nuclear matter. Nevertheless, the curve falls off much faster with decreasing $\xi$ and coincides with the DD-ME2 line at $T_{\rm CM}$=0. For comparison also recent results from chiral perturbation theory (ChPT) by Fiorilla et.al. [48] are displayed. In this calculation the one- and two-pion exchange diagrams as well as $\Delta$-isobar degrees of freedom are explicitly taken into account. In Table IV we provide a summary of the results for some fixed values of the proton-neutron asymmetry $\xi$. It is remarkable that the DDRH result is very close to the one of ChPT throughout the whole $\xi$ range. This indicates that in the DDRH the higher order correlation effects on the isospin degree of freedom are implicitly included in the density dependent terms of the isovector-vector and isovector-scalar channels.

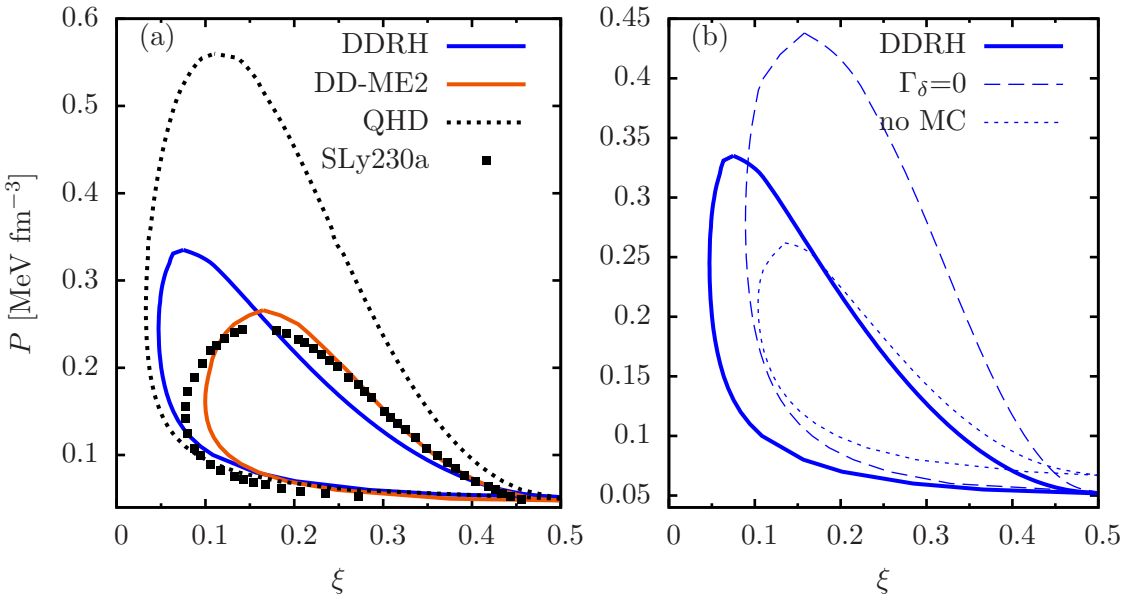


Figure 22: (Color online) (a) Comparison of the binodal surface at $T$=10 MeV between the DDRH, DD-ME2, QHD and SLy230a [10] model. (b) Results of calculations without $\delta$ meson interaction (dashed) and without momentum correction (short dashed) are compared to the full DDRH calculation.

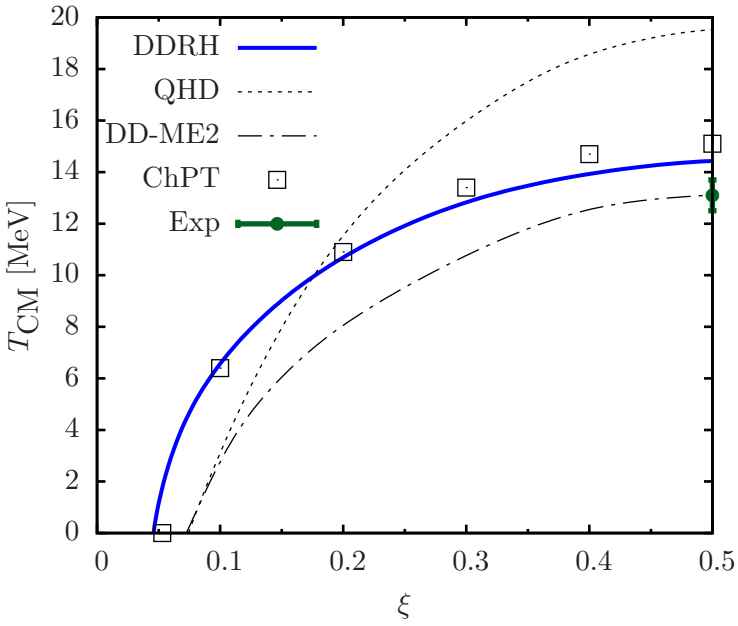


Figure 23: (Color online) The critical temperature of mechanical instability as a function of the proton fraction $\xi$. The results are compared between different models. The good agreement between our DDRH and the ChPT results of [48] is remarkable

## VI. SUMMARY AND OUTLOOK

The equation of state of asymmetric nuclear matter was studied in the microscopic DDRH approach. The approach, being based on a Dirac-Brueckner approach to in-medium interactions, incorporates the essential aspects of an *ab initio* description by relying only on a free-space $NN$-interaction but deriving the medium-dependent modifications in a self-consistent manner. An important step is the projection of the medium dependence onto effective

Table IV: Comparison of the critical temperatures, $T_{\rm CM}$ [MeV], at different asymmetry values $\xi$ .

| $\xi$ | DDRH | DD-ME2 | ChPT |
|---|---|---|---|
| 0.5 | 14.6 | 13.3 | 15.1 |
| 0.4 | 14.0 | 12.6 | 14.7 |
| 0.3 | 12.8 | 10.8 | 13.4 |
| 0.2 | 10.7 | 8.1 | 10.8 |
| 0.1 | 6.6 | 2.6 | 6.5 |

density dependent meson-baryon interactions leading to the formulation of relativistic nuclear field theory with vertex functionals depending on the field operators. As discussed above, in mean-field approximation the field theoretical functionals become functions of the nuclear density. The mean-field limit is treated as the leading order term in an expansion around the ground state expectation value of a given configuration of symmetric or asymmetric nuclear matter. While in former DDRH-related work investigations of cold nuclear and hypernuclear matter and applications to neutron stars and finite nuclei and hypernuclei were considered, in this paper we have applied the approach for the first time to nuclear matter at finite temperature $T > 0$. The nuclear equation of state was investigated in relativistic mean-field approximation for proton ratios $\xi = Z/A$ ranging from symmetric nuclear matter ($\xi = \frac{1}{2}$) to pure neutron matter ($\xi = 0$).

As a generic feature of the DDRH theory we have included for the first time also isovector-scalar fields, realized in nature by the $a_0(980)$ meson. Already by general symmetry arguments this interaction channel must be included into the theory. The most important effect is that in asymmetric nuclear matter protons and neutrons obtain different relativistic effective masses. Hence, the two species of nucleons become mechanically distinguishable, affecting directly the thermodynamical properties. Of particular importance is the quite different behavior of asymmetric matter at the phase boundaries.

Although there exist quite a number of studies on the thermodynamics of symmetric nuclear matter and pure neutron matter, much less attention has been paid on the properties of warm asymmetric nuclear matter. While symmetric nuclear matter can still be considered as a single-component Fermi gas this is no longer possible in asymmetric nuclear matter. Unequal proton and neutron numbers are translating into differences in Fermi momenta and chemical potentials, thus changing the chemical composition and kinetic and, due to isovector interactions, the mechanical properties of the protons and neutrons, hence making the two species thermodynamical distinguishable. Thus, as discussed in the previous sections a much more involved theoretical treatment in terms of a two-component Fermi gas is required. The increased theoretical effort, however, is awarded by a much richer phase structure of asymmetric nuclear matter. As discussed in detail in section III the phase structure of asymmetric nuclear matter is conveniently studied in terms of the total, isoscalar, and the isovector baryon chemical potentials, respectively, accounting for the conserved charges of the system, namely the total baryon number $B$ and the third component $I_3 \sim \frac{\rho_n - \rho_p}{\rho}$ of the total isospin, which is synonym to the conservation of the total charge of the system. Against naïve first expectations, it is not the number of protons and neutrons separately which is conserved, but the overall Noether-charges are the conserved quantities. This is seen clearly at the phase transition boundaries: during the phase transition the baryonic composition might change as long as $B$ and $I_3$ are conserved. As pointed out, the density dependence and isospin structure of the in-medium interactions plays a crucial role for the thermodynamics of warm asymmetric nuclear matter, affecting directly the details of the phase structure of the system. These aspects were studied in due detail by comparing our fully microscopic DDRH results with results obtained with the purely phenomenological RMF-approaches like the original scalar-vector model of Serot and Walecka and the density dependent extensions as the DD-ME2-approach of Ring *et al.*. Qualitatively, the three approaches lead to similar predictions on the thermodynamics of warm nuclear matter, but in detail the differences in nuclear dynamics are reflected by variations in the phase diagrams. The positive message of that comparison is that models describing cold nuclear matter properly are also close in their predictions for warm nuclear matter, at least in the temperature range below $t \sim 100$ MeV and a compression factor of up to two or three times nuclear saturation density. This result is certainly of interest for heavy ion physics because it confirms and gives further confidence to the widely used treatment of heavy ion collisions in terms of a transport theoretical description based on RMF-type dynamics.

Clearly, the approach presented here is open to further extensions. The inclusion of hyperons is one of the interesting cases allowing to study warm hypermatter. Adding in addition beta-equilibrium one will be able to describe warm neutron star matter thus giving access to a more extended, new approach to the early stages of a neutron star just after the formation of a proto-neutron star and the subsequent cooling phase.

*Acknowledgements:* This work was supported in part by DFG Graduiertenkolleg Giessen-Kopenhagen-Helsinki *Complex Systems of Hadrons and Nuclei*, GSI Darmstadt, and Helmholtz Graduate School for Hadron and Ion

Research.


[1] G. Sauer, H. Chandra, and U. Mosel, Nuclear Physics A **264**, 221 (1976).
[2] B. Friedman and V. R. Pandharipande, Nucl. Phys. A **361**, 502 (1981).
[3] M. Baldo and L. S. Ferreira, Phys. Rev. C **59**, 682 (1999).
[4] H. A. Weldon, Phys. Rev. D **26**, 1394 (1982).
[5] R. J. Furnstahl and B. D. Serot, Phys. Rev. C **41**, 262 (1990).
[6] W. Botermans and R. Malfliet, Phys. Rep. **198**, 115 (1990).
[7] B. ter Haar and R. Malfliet, Phys. Rev. Lett. **56**, 1237 (1986).
[8] B. ter Haar and R. Malfliet, Phys. Rev. Lett. **59**, 1652 (1987).
[9] H. Müller and B. D. Serot, Phys. Rev. C **52**, 2072 (1995).
[10] M. Dutra, O. Lourenço, A. Delfino, J. S. Sá Martins, C. Providência, S. S. Avancini, and D. P. Menezes, Phys. Rev. C **77**, 035201 (2008).
[11] S. L. Shapiro and S. A. Teukolsky, *Black Holes, White Dwarfs, and Neutron Stars* (Wiley-VCH Verlag GmbH, Weinheim, Germany, 1983).
[12] P. Gögelein, E. N. E. v. Dalen, C. Fuchs, and H. Müther, Phys. Rev. C **77**, 025802 (2008).
[13] T. Gaitanos, H. Lenske, and U. Mosel, Progress in Particle and Nuclear Physics **62**, 439 (2009), ISSN 0146-6410, heavy-Ion Collisions from the Coulomb Barrier to the Quark-Gluon Plasma 30th Course International Workshop on Nuclear Physics.
[14] T. Gaitanos, A. Larionov, H. Lenske, and U. Mosel, Nucl.Phys. **A881**, 240 (2012), 1111.5748.
[15] J. Bondorf, A. Botvina, A. Ilinov, I. Mishustin, and K. Sneppen, Phys.Rept. **257**, 133 (1995).
[16] H. Lenske and C. Fuchs, Phys. Lett. B **345**, 355 (1995).
[17] C. Fuchs, H. Lenske, and H. H. Wolter, Phys. Rev. C **52**, 3043 (1995).
[18] F. Hofmann, C. M. Keil, and H. Lenske, Phys. Rev. C **64**, 034314 (2001).
[19] F. de Jong and H. Lenske, Phys. Rev. C **58**, 890 (1998).
[20] H. Lenske, Lect. Not. Phys., Springer, Berlin-New York **641**, 147 (2004).
[21] T. Gaitanos, M. D. Toro, S. Typel, V. Baran, C. Fuchs, V. Greco, and H. Wolter, Nuclear Physics A **732**, 24 (2004).
[22] E. N. E. van Dalen and H. Müther, Phys. Rev. C **87**, 024317 (2013).
[23] N. M. Hugenholtz and L. van Hove, Physica **24**, 363 (1958).
[24] G. A. Lalazissis, T. Nikšić, D. Vretenar, and P. Ring, Phys. Rev. C **71**, 024312 (2005).
[25] G. A. Lalazissis, J. König, and P. Ring, Phys. Rev. C **55**, 540 (1997).
[26] B. D. Serot, Physics Letters B **86**, 146 (1979).
[27] E. Chabanat, P. Bonche, P. Haensel, J. Meyer, and R. Schaeffer, Nuclear Physics A **627**, 710 (1997), ISSN 0375-9474.
[28] B. D. Serot and J. D. Walecka, *The Relativistic Nuclear Many Body Problem*, vol. 16 (Advances in Nuclear Physics, 1986).
[29] M. Anastasio, L. Celenza, W. Pong, and C. Shakin, Phys. Rep. **100**, 327 (1983).
[30] C. Horowitz and B. Serot, Nucl. Phys. A **464**, 613 (1987).
[31] B. ter Haar and R. Malfliet, Phys. Rep. **149**, 207 (1987).
[32] R. Brockmann and R. Machleidt, Phys. Rev. C **42**, 1965 (1990).
[33] H. F. Boersma and R. Malfliet, Phys. Rev. C **49**, 233 (1994).
[34] H. Huber, F. Weber, and M. K. Weigel, Phys. Rev. C **51**, 1790 (1995).
[35] W. Kohn and L. Sham, Phys. Rev. A **140**, 1133 (1965).
[36] P. Hohenberg and W. Kohn, Phys. Rev. B **136**, 864 (1964).
[37] R. Brockmann and H. Toki, Phys. Rev. Lett. **68**, 3408 (1992).
[38] S. Typel and H. Wolter, Nuclear Physics A **656**, 331 (1999).
[39] A. L. Fetter and J. D. Walecka, *Quantum Theory of Many-Particle Systems* (McGraw-Hill Publishing Company, 1971).
[40] J. I. Kapusta and C. Gale, *Finite-Temperature Field Theory* (Cambridge University Press, 1989).
[41] F. Sammarruca, Journal of Physics G: Nuclear and Particle Physics **37**, 5105 (2010).
[42] V. A. Karnaukhov, H. Oeschler, A. Budzanowski, S. P. Avdeyev, A. S. Botvina, E. A. Cherepanov, W. Karcz, V. V. Kirakosyan, P. A. Rukoyatkin, I. Skwirczyńska, et al., Physics of Atomic Nuclei **71**, 2067 (2008).
[43] T. Nikšić, D. Vretenar, and P. Ring, Phys. Rev. C **66**, 064302 (2002).
[44] H. Jaqaman, A. Z. Mekjian, and L. Zamick, Phys. Rev. C **27**, 2782 (1983).
[45] G. Peilert, H. Stocker, and W. Greiner, Rep. Prog. Phys. **57**, 533 (1994).
[46] A. Rios, A. Polls, and I. Vidaña, Phys. Rev. C **79**, 025802 (2009).
[47] M. Dželalija, N. Cindro, Z. Basrak, R. Čaplar, S. Hölbling, M. Bini, P. Maurenzig, A. Olmi, G. Pasquali, G. Poggi, et al., Phys. Rev. C **52**, 346 (1995).
[48] S. Fiorilla, N. Kaiser, and W. Weise, Nuclear Physics A **880**, 65 (2012).
[49] B.-A. Li, L.-W. Chen, and C. Ko, Physics Reports **464**, 113 (2008).
[50] H.-T. Janka, K. Langanke, A. Marek, G. Martínez-Pinedo, and B. Müller, Physics Reports **442**, 38 (2007).
[51] L. F. Roberts, G. Shen, V. Cirigliano, J. A. Pons, S. Reddy, and S. E. Woosley, Phys. Rev. Lett. **108**, 061103 EP (2012).
[52] R. Wada, K. Hagel, L. Qin, J. Natowitz, Y. Ma, G. Röpke, S. Shlomo, A. Bonasera, S. Typel, Z. Chen, et al., Phys. Rev. C **85**, 064618 (2012).

[53] D. T. Khoa and H. S. Than, Phys. Rev. C **71**, 044601 (2005).
[54] R. Furnstahl, Nuclear Physics A **706**, 85 (2002), ISSN 0375-9474.
[55] D. V. Shetty, S. J. Yennello, and G. A. Souliotis, Phys. Rev. C **76**, 024606 (2007).
[56] W. Qian, R.-K. Su, and P. Wang, Physics Letters B **491**, 90 (2000).
[57] J. M. Lattimer and D. G. Ravenhall, Astrophysical Journal **223**, 314 (1978).
[58] C. Ducoin, P. Chomaz, and F. Gulminelli, Nuclear Physics A **771**, 68 (2006).
[59] G.-H. Zhang and W.-Z. Jiang, Physics Letters B **720**, 148 (2013).
[60] H. Huber, F. Weber, and M. K. Weigel, Phys. Rev. C **57**, 3484 (1998).
[61] P. Sahu, T. Jha, K. Panda, and S. Patra, Nucl. Phys. A **733**, 169 (2004).